POLITECNICO DI MILANO

SCUOLA DI INGEGNERIA INDUSTRIALE E DELL'INFORMAZIONE
CORSO DI LAUREA MAGISTRALE IN INGEGNERIA BIOMEDICA

CORRELATION BETWEEN GRAY MATTER ATROPHY IN SEGMENTED CORTEX AREAS AND WHITE MATTER DAMAGE FROM PROBABILISTIC TRACTS IN MULTIPLE SCLEROSIS

Relatori:
Prof. GIUSEPPE BASELLI
Dr. NIELS PETER BERGSLAND

Tesi di Laurea di:
NICOLA ANDREA CALDERISI
Matr. 820692

ANNO ACCADEMICO
2014/2015

Bisognerebbe rendere tutto il più semplice possibile
ma non troppo semplice (A. Einstein).

TABLE OF CONTENTS

LIST OF FIGURES

LIST OF TABLES

LIST OF ABBREVIATIONS

AD	Axial diffusivity
ADC	Apparent Diffusion Coefficient
ANCOVA	ANAlysis of COVAriance
ATR	Anterior Thalamic Radiation
BEDPOST	Bayesian Estimation of Diffusion Parameters Obtained using Sampling Techniques
CNS	Central Nervous System
CSF	CerebroSpinal Fluid
CST	CorticoSpinal Tract
DTI	Diffusion Tensor Imaging
DW	Diffusion-Weighted
DWI	Diffusion-Weighted Imaging
EPI	Echo Planar Imaging
FA	Fractional Anisotropy
GM	Gray Matter
HBP	Human Brain Project
HC	Healthy Controls
HCP	Human Connectome Project
ILF	Inferior Longitudinal Fasciculus
MCMC	Markov Chain Monte Carlo
MD	Mean Diffusivity

MLR	Multiple Linear Regression
MNI	Montreal Neurological Institute
MPRAGE	Magnetization-Prepared Rapid Gradient Echo
MS	Multiple Sclerosis
MRI	Magnetic Resonance Imaging
MRS	Magnetic Resonance Spettroscopy
N	Number
NAWM	Normal Appearing White Matter
PAC	Primary Auditory Cortex
PD	Proton Density
PMC	Primary Motor Cortex
RD	Radial Diffusivity
RRMS	Relapsing-Remitting Multiple Sclerosis
SLFP	Superior Longitudinal Fasciculus-Parietal endings
SLFT	Superior Longitudinal Fasciculus-Temporal endings
SM	Sclerosi Multipla
SP	Secondary Progressive
SNC	Sistema Nervoso Centrale
SPM	Statistical Parametric Mapping
TE	Time Echo
TIV	Total Intracranial Volume
TRACULA	TRActs Constrained by the UnderLying Anatomy
UNC	UNCinate fasciculus
VBM	Voxel Based Morphometry
WM	White Matter

SOMMARIO

Introduzione e obiettivi dello studio: La sclerosi multipla (SM) è una malattia cronica autoimmune che affligge il sistema nervoso centrale (SNC) e che tipicamente colpisce i giovani causando deficit cognitivi nonché numerosi disturbi ai sistemi visivo, sensoriale e motorio. Sebbene storicamente l'interesse della comunità scientifica si sia focalizzato sullo studio del deterioramento della materia bianca, caratterizzato da perdite di mielina e dal danneggiamento degli assoni, le patologie della materia grigia, evidenziate in primis dall'atrofia di svariate aree funzionali, stanno progressivamente diventando un argomento di ricerca fondamentale per capire il meccanismo patologico alla base della SM. Ad oggi un numero sempre maggiore di ricercatori ha applicato le tecniche di *magnetic resonance imaging* (MRI) allo studio delle presunte relazioni tra l'atrofia della materia grigia e la degenerazione della materia bianca, tuttavia focalizzandosi soprattutto solo su singole connessioni (e.g. singolo tratto di materia bianca e area(e) associata(e) e/o valutazioni statistiche della quantità di materia grigia, come, ad esempio, nel caso della *voxel based morphometry*). Rispetto a quanto già stato fatto in passato, nel corso di questo lavoro sono state utilizzate tecniche avanzate di MRI per approfondire la conoscenza delle relazioni esistenti tra la patologia della materia grigia e i compartimenti di materia bianca a essa associati nei pazienti affetti da SM. Nello specifico, sono state analizzate le correlazioni tra sei principali tratti di materia bianca e lo spessore di quelle regioni di corteccia coinvolte nei loro circuiti cognitivi, sensoriali o motori.

Materiali e Metodi: Nello studio sono stati coinvolti 32 pazienti con sclerosi multipla recidivante remittente (RRMS) e 30 pazienti sani, in veste di controlli. Nello specifico, si è utilizzato il software *FreeSurfer* per ottenere la segmentazione e la topografia precisa della corteccia e per ricavare misure, specifiche per ogni paziente, dello spessore corticale e dell'area superficiale. TRACULA, (TRActs Constrained by the UnderLying Anatomy), un innovativo algoritmo probabilistico che combina

informazioni anatomiche a tecniche di *diffusion tensor imaging* (DTI) multi compartimentale, è stato successivamente utilizzato per ricostruire sei principali tratti della materia bianca: le radiazioni talamiche anteriori (ATR), il tratto corticospinale (CST), il fascicolo longitudinale inferiore (ILF), due porzioni del fascicolo longitudinale superiore, i.e. le sue terminazioni parietali e temporali (SLFP and SFLT, rispettivamente) e il fascicolo uncinato (UNC). Una scrupolosa analisi della letteratura, confermata da un metodo da noi sviluppato, ha poi permesso di scegliere quale regione della corteccia associare a ciascun tratto in base ai circuiti funzionali di cui fanno parte. Tramite TRACULA sono state ottenute misure specifiche di diffusività assiale (AD), diffusività radiale (RD), diffusività media (MD) e anisotropia frazionale (FA) relative ai sopracitati fasci di materia bianca. Modelli di analisi della covarianza (ANCOVA), controllando per età e sesso, sono stati utilizzati per valutare eventuali differenze significative fra il gruppo di controllo e i pazienti affetti da SM, sia per le misure morfologiche riguardanti la corteccia che per le misure derivanti dalla DTI. Età e sesso sono state anche utilizzate come covariate anche per analizzare le correlazioni parziali tra i parametri DTI e le misure corticali delle regioni associate. Per omogeneità di confronto, le stesse analisi sono state condotte per ogni tratto con un'area della corteccia a esso non connesso. Infine, si è fatto ricorso a modelli di regressione lineare multipla (MLR) per predire lo spessore di una zona della corteccia a partire dagli indici DTI sia di un tratto a essa connesso sia da uno a essa non connesso.

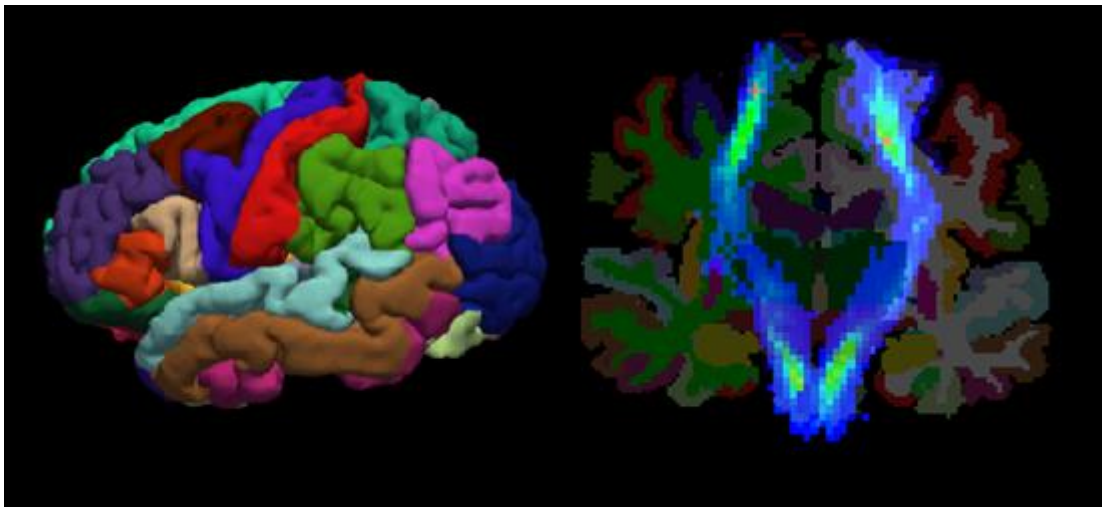

Figura 1 Esempio di parcellazione della corteccia e della ricostruzione del tratto corticospinale in un soggetto rappresentativo del presente studio

Risultati: Nella figura 1 viene mostrato un esempio della parcellizzazione della corteccia e della successiva ricostruzione del tratto corticospinale di un soggetto in esame. Nei pazienti affetti da RRMS sono stati riscontrati rispetto al gruppo di controllo valori maggiori di AD, MD e RD e valori minori di FA, di spessore della corteccia e di area superficiale. Sorprendentemente, il parametro FA si è rivelato essere il parametro meno sensibile, soprattutto se paragonato al MD, confermando che il meccanismo che porta al danno microstrutturale non è stato ancora compreso pienamente. Sono state riscontrate da un minino di una a un massimo di tre correlazioni significative tra i quattro parametri DTI di ogni tratto e le misure morfologiche strutturali delle rispettive regioni corticali. Per quanto riguarda il confronto con la regione non connessa, non sono state trovate invece correlazioni per il CST, il SLFP e l'UNC, mentre una correlazione è stata evidenziata per l'ATR e il SLFT e, infine, due correlazioni per l'ILF. In tutte le regressioni lineari multiple sono stati inclusi nel modello predittivo dello spessore di una zona della corteccia, oltre all'età, solo parametri DTI appartenenti al tratto connesso a tale regione e mai parametri di un tratto non connesso.

Discussione e conclusioni: Il risultato di questo studio evidenza l'importanza della connettività anatomica e funzionale che vi è tra specifici tratti di materia bianca e le rispettive regioni corticali di materia grigia nella diffusione della degenerazione che caratterizza la SM. Quanto appena detto viene corroborato tanto dalle correlazioni trovate quanto dai risultati dei modelli di MLR. Saranno comunque necessarie successive analisi e studi longitudinali per poter comprendere più a fondo il meccanismo patogeno che causa l'atrofia della materia grigia e il danno della materia bianca nei pazienti con SM. Tali studi permetterebbero anche di migliorare la differenziazione del danno specifico da quello diffuso, e di caratterizzare la relazione temporale (o, ancor di più, causale) che vi è tra il danno nella materia bianca e le mancanze strutturali e funzionali della materia grigia.

SUMMARY

Background and purpose: Multiple sclerosis (MS) is a chronic inflammatory, immune mediated disease affecting the central nervous system (CNS) that typically affects young adults leading to impairments in motor, visual, sensory and cognitive functions. While historically much emphasis was placed on studying white matter (WM) injury, characterized by demyelination and axonal transection, the gray matter (GM) pathology, primarily evidenced by cortical atrophy of several functional areas, is gaining more and more attention as a fundamental research focus in understanding the pathogenic mechanism of MS. In this framework, the attention of research is moving towards the contemporary study of GM and WM degeneration in MS patients. Several magnetic resonance imaging (MRI) studies have already investigated the presumed relationship between GM atrophy and WM pathology, but mostly focused only on individual connections (i.e. single WM tract and associated GM area(s)) and/or fuzzy statistical evaluations of GM quantity, as in voxel based morphometry. Against this background, the current work used advanced MRI technique to gain deeper insights into the relationship between pathology in the GM and connected WM compartments in patients with MS. In particular, we studied the correlations of six major WM tracts with the cortical thinning of those regions of the cortex that are involved in their cognitive, sensory or motor circuits.

Materials and methods: This study included thirty-two patients with relapsing-remitting multiple sclerosis (RRMS) and thirty healthy controls (HC). In particular we used FreeSurfer to obtain precise cortex segmentation and topology, hence deriving subject- and location-specific measures of cortical thickness and surface area. TRACULA (TRActs Constrained by the UnderLying Anatomy), a novel probabilistic tractographic algorithm that combines anatomical priors with multi-compartmental diffusion tensor imaging (DTI), was then used to reconstructs six major WM pathways: the anterior thalamic radiations (ATR), the corticospinal tract (CST), the

inferior longitudinal fasciculus (ILF), two portion of the superior longitudinal fasciculus, i.e. the parietal and the temporal endings (SLFP and SFLT, respectively) and the uncinate fasciculus (UNC). An attentive analysis of the literature confirmed by an in-house method allowed us to choose which region of the cortex to associate to each tract according to the functional circuits in which they are involved. Individual measures of axial diffusivity (AD), radial diffusivity (RD), mean diffusivity (MD) and fractional anisotropy (FA) were obtained from the aforementioned WM bundles. Significant differences were evaluated between RRMS and HC groups with analysis of covariance (ANCOVA) models, controlling for age and sex. Age and sex were also used as covariates when testing for partial correlation between the DTI measures of each tract and the cortical measures of the associate region of the cortex. The same analyses were conducted on each tract with a non-connected regions of the cortex for the sake of comparison. Finally, multiple linear regressions (MLRs) were conducted predicting the cortical thickness of a region of the cortex from the DTI measures of a connected and a non-connected tract.

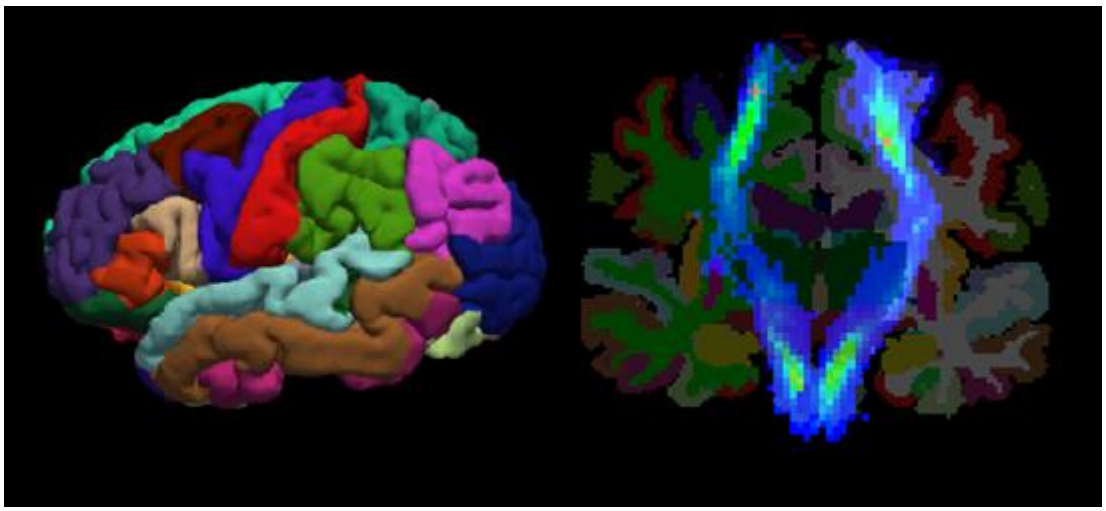

Figura 2: Example of the parcellation of the cortex and of the probabilistic reconstruction of the corticospinal tract in a representative subject of the current study

Results: An example of a subject-specific cortical parcellation and of a reconstructed tract are shown in figure 1. RRMS patients presented with increased AD, MD and RD and decreased FA, cortical thickness and surface area with respect to the control group. Interestingly, FA was unexpectedly the least sensitive index, while MD was the main

one, thus confirming that the underlying micro-structural damage mechanism are neither trivial nor fully understood. A minimum of one and a maximum of three significant correlations were found between the four DTI measures from each tract and the morphologic measure from associated regions of the cortex. Regarding the comparison with a non-connected region no correlations were found for the CST, the SLFP and the UNC, while one was found for the ATR and the SLFT and two for the ILF. Each MLR performed retained in the final model age and one DTI index of the connected tract as predictive variable of the cortical thickness of a region, excluding the other DTI indexes of that tract and all the indexes of the non-connected tracts.

Discussion and conclusion: The results of the present study highlight the importance of the anatomical and functional connectivity between specific WM tracts and the connected GM cortical regions, though in the framework of the widespread damage that characterizes the MS disease. This notion is corroborated by both the correlations found and the MLR performed. Further analyses and longitudinal studies are needed to better understand the pathogenic mechanism that cause the contemporary GM atrophy and WM injury in MS patients, to improve the differentiation of specific from generalized damage, and to characterize the temporal (or even causal) relationship between WM and GM structural and functional losses.

INTRODUCTION

This work used advanced magnetic resonance imaging (MRI) techniques to shed light on the role of local gray matter (GM) and white matter (WM) connections in multiple sclerosis (MS), a neurological disease causing widespread damage throughout the central nervous system.

Structural connectivity in the brain

The brain is the most complex organ of the human body and probably one of the most complicated systems in nature. It is a highly efficient integrative system, as it combines information arriving from both different districts of the body and the external environment to provide cognitive/motivational processes as well as motor actions. Information is very rapidly carried via the WM fibers, organized into tracts, from one region of GM to another. In the last decades, the evidences of the existence of neuronal networks and the increase of knowledge about brain area specialization, have led the scientific community to consider the issue of brain connectivity as a topic of great relevance.

Brain connectivity studies aim at deeply exploring the intricate relation among regions which are strongly interconnected (Sporns et al., 2004). We can refer to brain connectivity at different levels: between single neurons (Hellwig et al., 2000; Thomas et al., 1984; Dickson et al.; 1974; Michalski et al., 1983), between neuronal population (K Sameshima et al., 1999; Boahen et al., 2000) or between anatomically segregated regions (Rubinov et al., 2010; Sporns et al., 2002). Furthermore, according to the types of connections, brain connectivity may be described as being anatomical/structural (i.e., anatomical links, such as fiber pathways) or functional (i.e., the correlations between GM regions, which are attributed a functional meaning). Since the approach of this work is structural, only the former connectivity aspect is

addressed by assessing the integrity of WM tracts in important cognitive, motor and somatosensory circuits.

Nonetheless, morphological GM aspects are focused as well and put in relation with the WM ones. Namely, the correlations between the GM atrophy and the damage of impinging WM tracts is evaluated in both MS patients and healthy controls.

The MRI technique that allows to study WM tracts is tractography, derived from diffusion-weighted imaging (DWI). Specifically, it allows for the virtual reconstruction of WM fiber bundles, making feasible *in-vivo* and *non-invasive* structural connectivity studies (Basser et al, 2000; Melhem et al., 2002; Catani et al., 2008). The first tractographic investigations were carried out at the end of the last century (Makris et al., 1997), taking advantage of the principles of water diffusion (i.e., Brownian motion) applied to brain micro-structures. Water diffusion, indeed, is hindered by anisotropic structures such as WM fibers, which constrain the water molecules to move along them. Thus following the water molecules represents an indirect way to follow the fibers and subsequently to reconstruct the underlying WM tracts. This technique stood for a real revolution in brain studies since WM had never been identified by any direct *in-vivo* inspection but exclusively by post-mortem brain dissections. Therefore, tractography allows nowadays a worthwhile estimation of the brain structural connectivity pattern.

All the considerations above have been the premises of innovative and ambitious projects such as the Human Connectome Project (HCP) (Elam et al., 2014; Van Essen et al., 2012;) and Human Brain Project (HBP) (Huerta et al., 1993; Koslow et al., 1997; Shepherd et al., 1998), whose challenging aim consists in the mapping of the whole brain functionality within the next ten years. In particular, the HCP appears extremely interesting and revolutionary since it has made high quality data available for the entire scientific community in order to promote brain connectivity studies with a multimodal approach (i.e., with images acquired with different techniques, such as resting state functional MRI, task-based functional MRI, DWI).

In this context the development of new tools for cortex segmentation and structure analyses reveals a striking breakthrough in the study of GM structure as well in its biological diversity and pathological modifications (Winkler et al., 2012; Chee et al., 2011; Dickerson et al., 2009).

Previous approaches to GM structural studies (mainly thickness) were necessarily poorly resolved, statistical, and population based, due to the high diversity of gyri and sulci patterns. E.g., the voxel based morphometry (VBM) approach (Celle et al.,2014; Scarpazza et al., 2015), smoothed out individual details by heavy low pass filtering and next used linear regression tools such as statistical parametric mapping (SPM) to study correlations with pathological or physiological conditions.

Conversely, the novel segmentation approaches yield a more precise mapping of the individual cortical areas than has been previously possible. This has been achieved due to the improved surface-based methodology, which overcomes some of the limitations inherent in traditional volumetric analyses. The "Theoretical Aspects" section of the text discusses these topics in more detail. Regardless, the improved approaches yield two key benefits: 1) crispy and individual cortex segmentations can be parceled in areas the structure of which is analyzed on a single subject basis; 2) a solid framework for the localization of tract probabilistic atlases is given on common landmarks. Both results are exploited in the present thesis in order to analyze the relationship between WM and GM damage in the main cognitive, motor and somatosensory circuits.

MS overview and relevance of MRI in MS studies

Since diffusion MRI was first introduced, many works have used DWI, and particularly diffusion tensor imaging (DTI), to study patients affected by MS.

MS is a chronic inflammatory, immune mediated, disease affecting the central nervous system (CNS) that typically affects young adults leading to impairments to motor, visual, sensor and cognitive functions (Liu et al., 2012). The disease is expressed in different clinical phenotypes, the most common of which is relapsing-remitting MS (RRMS), which is characterized by periodical relapses and remissions of neurological impairment. Then, a large portion of RRMS patients (30-40%) convert to secondary progressive (SP) MS within 10 years (Rovaris et al., 2006), which is characterized by a steady progression of neurological decline in the relative absence of relapses (Klaver et al., 2013).

WM studies in MS

The study of WM degeneration in MS is, historically, of great interest for researchers all over the world. Within the CNS, the immune system attacks myelin as well as the nerve fibers themselves, leading to demyelination and axonal transection (Kolasinski et al., 2012; Evangelou et al., 2000). MS autopsy studies report extensive signs of inflammation in the WM, including lymphocyte infiltration, complement deposition and blood-brain barrier disruption. (Bo et al., 2003; Brink et al., 2005; van Horssen et al., 2007). Then the damaged myelin forms scar tissue, called sclerosis, throughout the brain, giving the disease its name. When any part of the myelin sheath or nerve fiber is destroyed or even only damaged, neural impulses travelling along the axons are distorted or interrupted, leading to connectivity problems as an insufficient communication of different functional areas. This unbounded diffusion of the lesions and this inefficient networking, reported in MRI and magnetic resonance spectroscopy (MRS) studies in MS patients, unfortunately, makes the disease to cause symptoms that vary in a very wide range, with deficits of different neurosensory systems.

In this field an important place is occupied by diffusion weighted imaging (DWI), which leads to diffusion tensor imaging (DTI) and tractography, when analyzing anisotropic features over several directions Basser et al, 2000; Melhem et al., 2002; Catani et al., 2008. Thanks to this unique scope into the WM micro-structure, unresolved, though "statistically" assessed, the diffused WM damage, well beyond the radiologically contrasted lesions, was demonstrated, thus leading to the core concept of normally appearing WM (NAWM) [Mistry et al., 2013]. In the present work, however, average changes in DTI feature over entire tracts will be considered, whether the presence of lesions was evidence or not.

GM studies for MS

While much emphasis was historically placed on studying WM injury, the GM pathology is gaining more and more attention as a fundamental research focus in understanding the pathogenic mechanisms and the evolution of MS. In 1962, Brownell and Hughes described GM lesions in a selected set of MS autopsy cases. The authors used conventional immunohistochemistry and detected a total of 1595 lesions in 22

MS cases, of which 26% were located in the cortical GM or at the WM/GM border. Later studies, using more sensitive immunohistochemical staining, showed that GM demyelination was even more extensive. (Bo et al., 2003). In parallel, advances in MRI have enabled detection of changes in GM volume. (Audoin et al., 2004; Bozzali et al., 2002). However, the available imaging techniques are still unable to adequately detect GM lesions and/or microstructural damage in the cortex (Zivadinov et al., 2012; Hulst et al., 2011), both due to these lesions having a different underlying pathology compared with WM lesions and to the small volumes to be resolved; in fact, those in the GM appear to have minimal infiltration of immune cells and are of a less inflammatory nature (Hulst et al., 2011; Popescu et al., 2012; Bo et al., 2006). Nonetheless, studies in patients with RRMS showed that GM atrophy is a meaningful indicator of neurodegeneration and even a better indicator of disability progression than lesion burden (Fisher et al., 2008; Horakova et al., 2008; Tedeschi et al., 2009). Cognitive impairment in patients with RRMS is thought to be associated with MS-related GM pathology, particularly in the cortex (Calabrese et al., 2009), with variability in disability progression among patients with RRMS probably arising from differences in GM injury (Jure et al., 2010).

WM and GM studies in MS

In this framework, the attention of the research is moving towards the contemporary study of GM and WM degeneration in MS patients. Several MRI studies investigated the presumed relationship between GM atrophy and WM pathology. Most of these reported associations between GM loss and increased lesion load (Battaglini et al., 2009; De Stefano et al., 2003; Fisniku et al., 2008; Furby et al., 2009; Henry et al., 2008; Narayana et al., 2013; Roosendaal et al., 2011; Sailer et al., 2003; Tedeschi et al., 2005), and some additionally reported associations between atrophy and normal appearing tissue damage (Vrenken et al., 2006). Steenwijk et al. indicated that, in patients with long-standing MS, whole-brain and deep GM atrophy are associated with WM atrophy and lesion volume, while cortical atrophy is associated with normal appearing WM integrity loss (Steenwijk et al., 2014). To explore the spatial relationship between GM and WM, some authors investigated whether regional WM pathology is related to GM atrophy in specific regions. Using voxelwise statistics, they

found that regional GM atrophy could be better explained by WM pathology in connected areas compared to whole-brain measures (Sbardella et al., 2013, Boldini et al., 2009; Muhlau et al., 2013; Sepulcre et al.,2009). Only a few studies used a direct analysis of structural connectivity using DTI to assess the correlation between WM integrity and GM atrophy in connected areas (Henry et al., 2009; Jehna et al., 2013; Bergsland et al., 2015; Steenwijk et al., 2015). Those studies, which, however, focused mostly on specific GM regions and WM tracts, found a stronger relation between GM atrophy and WM lesions in connected rather than in non-connected areas. In particular, Bergsland et al. found that DTI measures relative to the integrity of the corticospinal tract (CST) correlated with the cortical thickness of a connected GM region, the primary motor cortex (PMC), while no associations were found with a non-connected cortical area such as the primary auditory cortex (PAC).

Aim of the work

Against this background, the present work was carried out to gain further insight into the relationship that exists between GM and WM in connected areas with respect to non-connected areas of the brain in MS disease. Unlike several previous studies, which were conducted only on overall GM-WM relationship or on individual GM-WM connections, we analyzed six WM fiber bundles and the associated areas of the cortex, aware of the widespread of the injury caused by MS in the whole brain.

In particular we used FreeSurfer 5.3 (Dale et al.,1999; Fischl et al., 1999, http://freesurfer.net/) and its tractography tool TRACULA (TRActrography Constrained by the UnderLying Anatomy, A. Yendiki et al., 2011, https://surfer.nmr.mgh.harvard.edu/fswiki/Tracula) to obtain cortical and DTI measures respectively.

FreeSurfer, as wider explained in 1.2, is an open source software suite for processing and analyzing human brain MRI images. Thanks to its processing stream, it allows to, among other functions, reconstruct the cortical surface, to parcellate the cortex and to estimate morphological measure of the latter such as cortical thickness and surface area (see 1.1). We used the *recon_all* tool of FreeSurfer to obtain the thickness and surface area measures of the following region of the cortex (referred to as “gyri” according to the segmentation operated by the tool): the caudal and the rostral

middle frontal gyri, the latero-orbital gyrus, the superior frontal gyrus, the precentral gyrus, the supramarginal and the superior parietal gyri, the lateral occipital gyrus, the middle and the inferior temporal gyrus and, finally, the superior temporal gyrus.

TRACULA, whose algorithm is depicted in 1.3.3, is a novel tractography algorithm for automated reconstruction of major WM pathways. It was used to reconstruct the anterior thalamic radiations (ATR), the CST, the inferior longitudinal fasciculus (ILF), two different portions of the superior longitudinal fasciculus (SLF), and the uncinate fasciculus (UNC) of 32 RRMS patients and 30 healthy controls (HC).

The aforementioned cortical regions and WM tracts were chosen after an attentive analysis of previous studies (Catani et al., 2012, Wakana et al., 2004, Catani et al., 2001, Burgel et al. 2005, Thiebaut de Schotten et al., 2010, Lawes et al., 2007, Felten et al., 2004, FitzGerald et al., 2002). These tracts, which play an important role in cognitive, somatosensory and motor processes, are all known to be affected by MS.

The ATR is a WM structure carrying fibers between thalamus and prefrontal cortex (referred to in the present work as "the caudal-rostral middle frontal gyri" according to the segmentation operated in FreeSurfer). ATR damages have a link with cognitive abnormalities (Mamah et al., 2009) and diffusivity changes have also been reported in schizophrenic (Oh et al., 2009) and stuttering patients (Watkins et al., 2008).

The CST is part of the pyramidal tracts; its fibers travel from the primary motor cortex (here "precentral gyrus") towards the spinal cord via the brainstem and are involved in the control of the movements of the body. Damages to the CST cause hemiparesis, hemiplegia as well as several other motor syndromes.

The ILF is the WM bundle considered to be the relay of visual information between the occipital (here "lateral occipital gyrus") and the temporal cortex (here "middle and inferior temporal gyri") involved in function as objects recognition and visual perception (Tusa et al., 1985). It was also demonstrated (Shinoura et al., 2010) that impairment of the ILF plays a role in visual memory disturbance as well as in almost the totality of the visual syndromes (Catani et al., 2012).

TRACULA (Yendiki et al., 2011) then reconstructs the SLF in two portions, the SLFP and the SLFT, according to Makris et al., 2005, both originating from the frontal cortex ("superior frontal gyrus" here) and ending in the parietal lobe ("supramarginal gyrus and superior parietal gyrus" here) and in the temporal lobe ("superior temporal

gyrus"), respectively. The SLFP transfers somatosensory information and damages could lead to tactile and visuospatial disease (Catani et al.,2012; Shinoura et el., 2009). The SLFT, also referred to as arcuate fasciculus, is involved in symbolic thought and memory syndromes and in other neuropsychiatric syndromes as dyslexia (Rimrodt et al., 2010).

Finally, the UNC is the WM fiber bundle that connects the frontal lobe ("lateral orbitofrontal gyrus") to the temporal one ("middle and inferior temporal giry"). It is involved in mnemonic and behavioral circuits, and its dysfunction could be linked to semantic dementia (Lainsey et al., 2011) and reduced verbal fluency (Papagno et al., 2011).

To conclude, we aimed to further inspect whether previous findings concerning the relevance of individual local GM-WM connections could be extended to connections in regions throughout the whole brain. Therefore, DTI indexes of integrity from the aforementioned WM tracts as the axial diffusivity (AD), the radial diffusivity (RD), the mean diffusivity (MD) and the fractional anisotropy (FA) (see 0) were put in relations with measures of GM atrophy, as thickness and surface area of both connected and non-connected regions of the cortex. Finally, we tested the relative importance of the local connections in predicting the thickness of an individual region of the cortex via multiple linear regression (MLR) approach.

1. THEORETICAL ASPECTS

1.1 **Contrast in MRI**

Image contrast is an important imaging parameter. It should be analyzed in its two basic aspects:

1) physical contrast attains to the measured property of the imaged object; revealed differences are expressed as contrast, which is the basis for the detection and recognition of structure; MRI deserves its popularity due to the wide range of special contrasts it offers, both anatomical and functional in nature;

2) visual contrast, is the consequence of the former, however, it is also conditioned by a proper choice of intensity scales appropriate to enhance recognition of the addressed details; importantly, the human visual system is better specialized in judging differences in intensity rather than absolute values of illuminance.

Technically, image contrast is defined in terms of difference in image intensity. In particular, let I_A be the intensity of tissue A, I_B be the intensity of tissue B, and C_{AB} be their contrast index. We have

$$\boldsymbol{C}_{AB} = \frac{|\boldsymbol{I}_A - \boldsymbol{I}_B|}{\boldsymbol{I}_{REF}} \tag{1.1}$$

where I_{REF} is a normalizing reference value. It is obvious from Eq. (1.1) that to enhance image contrast, one should maximize the differences in image intensity among different tissues.

In MRI, image intensity I is a multiparameter function; in fact it is a function of spin proton density ρ, relaxation times $T1$, $T2$ and $T2^*$, diffusion coefficient D, and so on. Thus, we can express the image contrast as

$$\boldsymbol{C}_{AB} \approx \boldsymbol{f}(\boldsymbol{\rho}, \boldsymbol{T1}, \boldsymbol{T2}, \boldsymbol{T2^*}, \boldsymbol{D}, \boldsymbol{v} \ldots) \tag{1.2}$$

where the exact functional form of "f" is dependent on the specific protocol or sequence design followed during the acquisition.

Indeed, the main advantage of MRI techniques is that one may chose the sequence parameters to decide, as a consequence, which information gather in the images according to the aim of the acquisition. Thus one may want to have a T1-weighted image contrast in a way that

$$\boldsymbol{C}_{\mathrm{AB}} \approx \boldsymbol{f}(\boldsymbol{\rho}, \boldsymbol{T1}) \tag{1.3}$$

or, similarly, a velocity-weighted MRI so that

$$\boldsymbol{C}_{\mathrm{AB}} \approx \boldsymbol{f}(\boldsymbol{v}) \tag{1.4}$$

and this is the case of the Magnetic Resonance Angiography (MRA).

Figure 1.1 displays some example concerning pure ρ (i.e., Proton Density, PD), T1 or T2 weighing, and MRA.

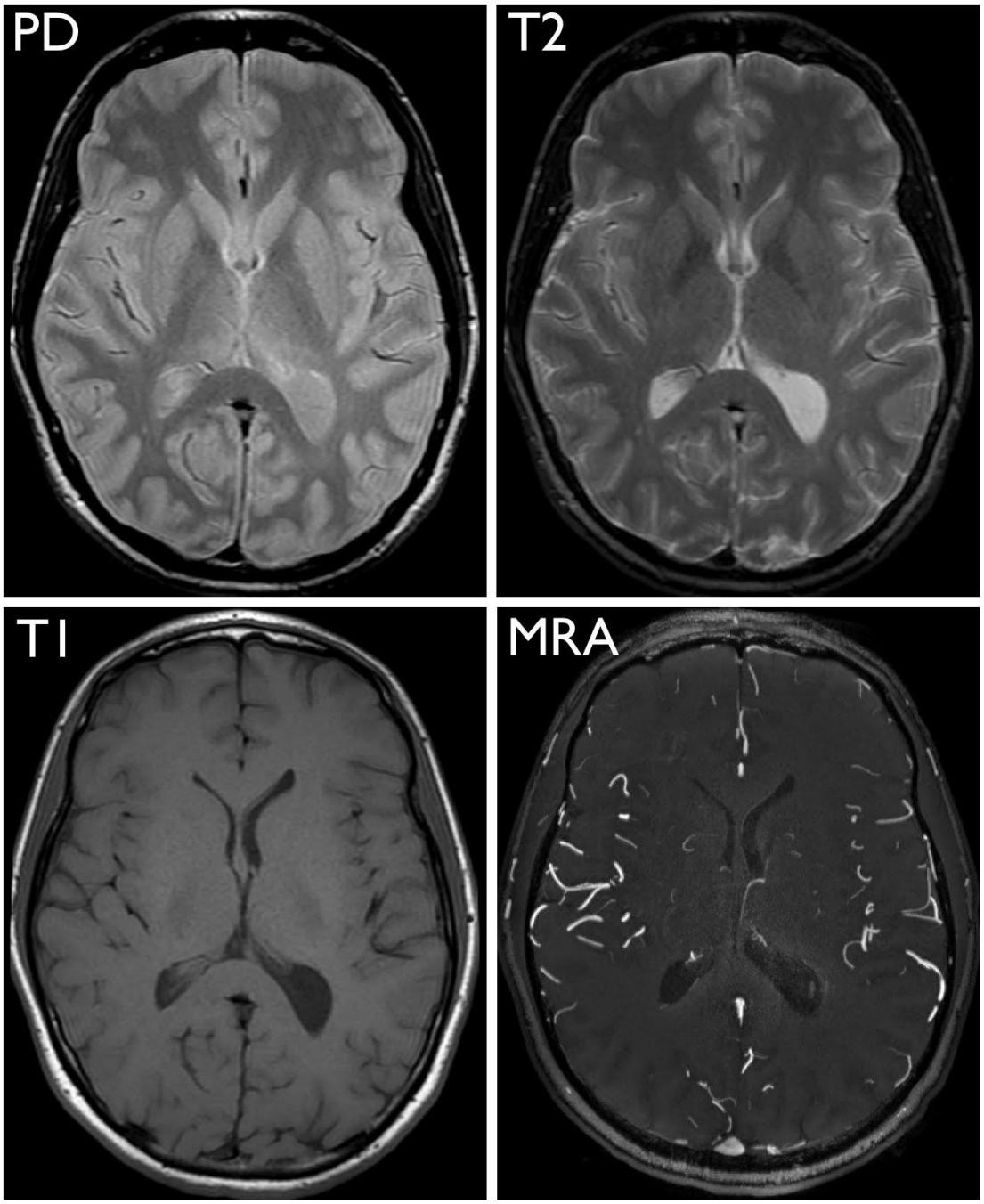

Figure 1.1: Different contrasts in MRI (http://www.radiology.ucsf.edu/)

1.2 **T1-weighted contrast: FreeSurfer pipeline and anatomical reconstructions**

Among the aforementioned different weightings of MRI contrast, T1-weighted contrast is the one that best fits the requirements for anatomical reconstruction This

contrast gives optimal differentiation between GM and WM due to T1 relaxation time that changes according to the amount of fat present in the tissue. Thus WM, which is rich in fat for the high presence of myelin, appears brighter (shorter T1, i.e. shorter saturation recovery) than GM that is characterized by a lower content of fat. (Figure 1.2). Therefore this the contrast we used as input to the FreeSurfer pipeline to obtain measures of cortical thickness and surface area.

FreeSurfer is a suite of tools for the analysis of neuroimaging data that provides a broad choice of algorithms to quantify the functional, connectional and structural properties of the human brain. It has evolved from a package primarily aimed at generating surface representations of the cerebral cortex into one that automatically creates models of most macroscopically visible structures in the human brain, starting from a T1-weighted input image (figure 1.2a). (Fischl et al., 2012)

1.2.1 *The surface-based stream*

In the cortical surface stream, the tools construct models of the boundary between WM and cortical GM as well as the pial surface, which corresponds to the boundary between the GM and the cerebrospinal fluid (CSF). First, the volume is registered through an affine registration with the Montreal Neurological Institute (MNI) atlas (Collins et al., 1994), which in its up-to-date version is also referred to MNI305, from the number of normal brains upon which its statistics is based. This will allow FreeSurfer to compute seed points in later stages. Then the B1 bias field (i.e., unwanted signal strength inhomogeneity) is estimated by measuring the variation in the WM intensity using the N3 algorithm. The main body of the WM is used to estimate the field across the entire volume. Voxels with highly probable WM classification are chosen based on their locations in MNI probabilistic map as well as on their intensity and the local neighborhood intensities. The intensity at each voxel is then divided by the estimated bias field at that location in order to remove the possible distortions due to the aforementioned bias.

After those preliminary operations on voxel intensity, the skull is stripped (figure 1.2b) using a deformable template model (Segonne et al., 2004). Then a WM mask is created, in which voxels are classified as WM or non-WM based on intensity and neighbor constraints (figure 1.3a). Cutting planes are chosen to separate the

hemispheres from each other as well as to remove the cerebellum and brain stem. The location of the cutting planes is based on the expected MNI location of the corpus callosum and pons, as well as several rule-based algorithms that encode the expected shape of these structures. An initial surface is then generated for each hemisphere by tiling the outside of the WM mass for that hemisphere. This initial surface is then refined to follow the intensity gradients between the white and gray matter and this is referred to as the "*white surface"* (figure 1.3b) (http://surfer.nmr.mgh.harvard.edu/fswiki/FreeSurferAnalysisPipelineOverview)

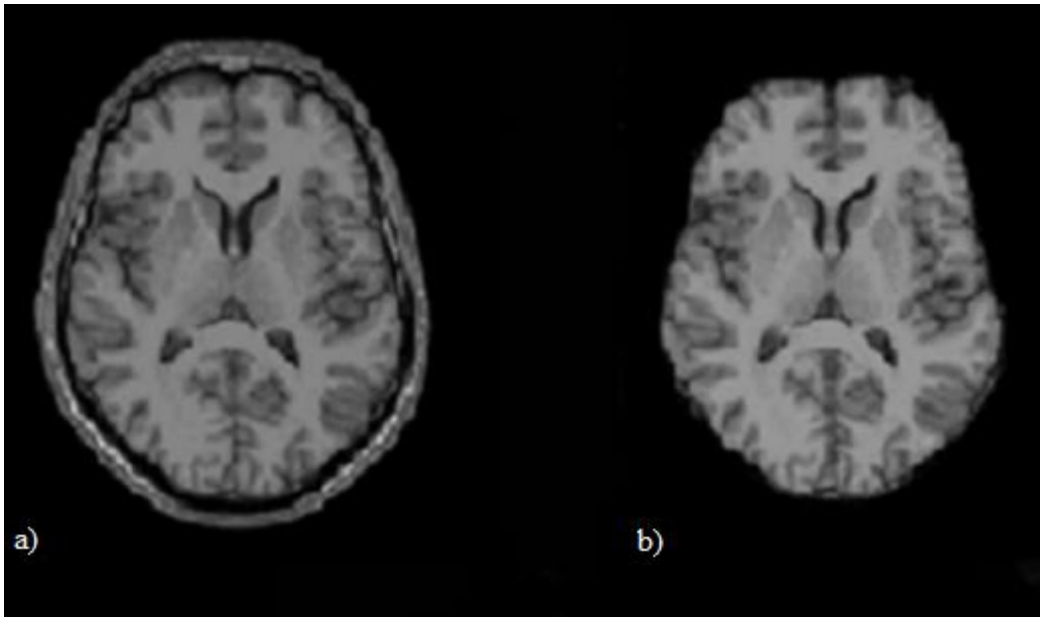

Figure 1.2 a) Axial view of a T1-weighted input image and b) the same slice after skull stripping. These images are taken from a representative subject of the present study.

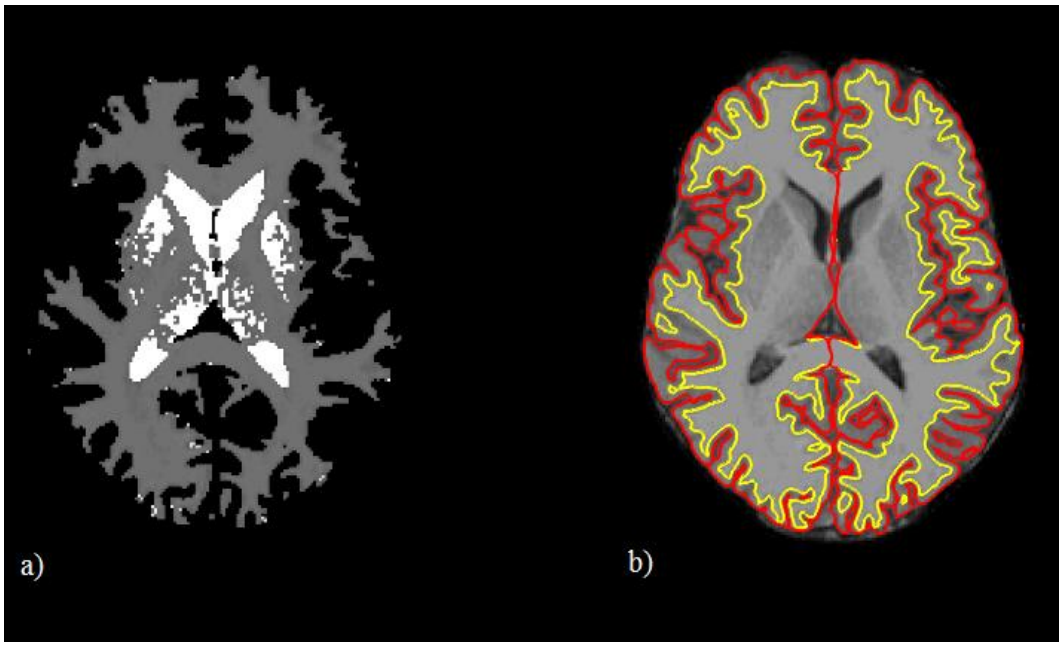

Figure 1.3 a) WM mask obtained classifying each voxel as WM/non-WM, according to their intensity and b) the white (yellow) and pial (red) surfaces overlaid on the original T1-weighed image. These images are taken from a representative subject of the present study.

1.2.2 *The volume-based stream*

The volume-based stream is designed to preprocess MRI volumes and label tissue classes. The stream consists of five stages, detailed description of which can be found in the literature (Fischl et al., 2002; Fischl et al., 2004). Although TRACULA internally uses elements of the volume-based stream, this feature is not in the scope of this work and will not be further described.

1.2.3 *Atlas construction: spherical coordinate system for the cortical surface*

In order to relate and compare anatomical features across subjects, it is necessary to establish a mapping that specifies a unique correspondence between each location in one brain and the corresponding location in another. Most comparisons of data across subjects in the human brain have relied on the 3-D normalization approach described by Talairach and Tournoux in 1988 and Talairach et al. in 1967. Although this type of approach has certain advantages (ease of use, widespread acceptance, applicability to subcortical structures), it also has significant drawbacks (Fischl et al., 1999). Limitations derive from the intrinsic topology of the cerebral cortex, which is a 2-D deeply folded sheet. For instance, estimates of the amount of “buried” cortex

range from 60–70% (Van Essen et al., 1997; Zilles et al., 1988). Thus distances measured in 3-D space between two points on the cortical surface will substantially underestimate the true distance along the cortical sheet, particularly in cases where the points lie on different banks of a sulcus. For example, the lateral tip of the central sulcus frequently lies within a centimeter of the superior temporal gyrus when the distance is measured in the Cartesian space. The distance between the same two points as measured along the actual cortical surface is 10 cm due to the depth of the Sylvian fissure (Fisch et al., 1999). This problem is compounded by the poor anatomical accuracy provided by the Talairach normalization approach. As numerous studies have demonstrated, the between-subject variability in the location of cortical anatomical landmarks after Talairach alignment is on the order of several centimeters (Steinmetz et al., 1984; Hunton et al., 1996; Thompson and Toga, 1996; Van Essen and Drury, 1997). Since many human functional areas (e.g., visual areas V2, V3, VP, V4v, MT1) are about 2 cm wide, the Talairach coordinate system does not have sufficient accuracy to differentiate neighboring cortical areas. This type of error makes it impossible to distinguish topographical and fine structural features of the cortical architecture based solely on Talairach coordinates (Fischl et al., 1999)

One of the main improvements offered by FreeSurfer is the use of a spherical coordinate system to map the surface of the brain (figure 1.4). This is possible because FreeSurfer cortical segmentation surface is vectorized and can be easily deformed to a topologically equivalent sphere. The reconstructed surface of each individual subject is first mapped onto a sphere, using a maximally isometric transformation (Fischl et al., 1998). The surfaces are then registered with an average, canonical surface, guided by a combination of folding-alignment (i.e. sulcus/gyrus). The canonical cortical surface is generated by combining multiple surfaces that have each been morphed into a parametric surface. A unified latitude and longitude system can then be established, allowing surface-based averages across subjects. As with the Talairach atlas, the coordinates of a single point (here latitude and longitude as opposed to the x,y,z coordinates) are used to index the corresponding point on each individual surface.

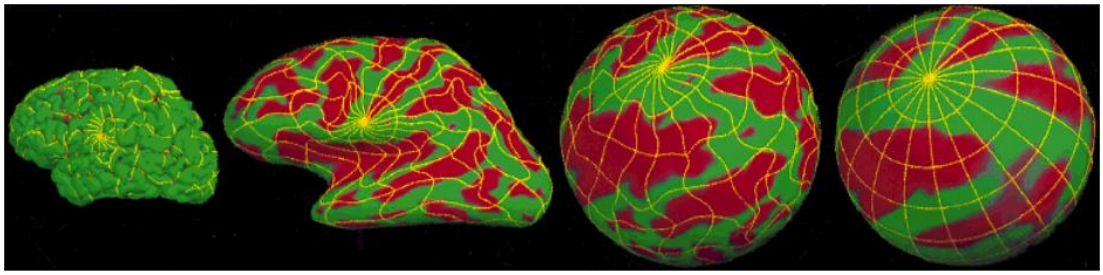

Figure 1.4 The leftmost image is the reconstruction of the pial surface (the boundary between gray and white matter) of an individual subject. This surface is then inflated to determine the large-scale folding patterns of the cortex (second image from left) and subsequently transformed into a sphere in a manner that minimizes metric distortion (third image from left). The folding patterns of the individual are then aligned with an average folding pattern (rightmost image). The natural coordinate system of the average surface can then be used to index any point on any of the surface representations of the individual. The coordinate lines painted onto the individual surfaces are no longer uniform; rather they occur at the same locations relative to the primary cortical folding pattern across all subjects.
Red and green regions represent sulci and gyri, respectively. (Fischl et al., 1999)

1.2.4 *Labeling a dataset*

So far we presented how univocally identify any point of the cortical surface in a spherical coordinate system.

The final segmentation for a given subject is based on both a subject-independent probabilistic atlas and subject-specific measured values. In the case of the former, the atlases are provided as part of the FreeSurfer package itself. These atlases have been constructed based on the manual labeling of the cortex in 3D T1-weighted images by expert readers. The local curvature is also measured at each vertex within the reconstructed cortex. Thus, the probabilistic atlases and subject-specific measures are used in an iterative process to label each cortical area. Further details are given below.

Three types of probabilities are computed at each point in the training set. First, the probability that the point x_i belongs to each of the label classes a_n (with n = 1,…,N) is computed.

$$p(x_i = a_n) \tag{1.5}$$

The second type of probability is computed from the spatial configuration of labels that exist in the training set, which is termed the neighborhood function. The neighborhood function is the probability that a given point x_i belongs to a label classes a_n given the classification of its neighboring points x_j (with j ≠ i and m = 1,…,N).

$$p(x_i = l_n \mid x_j = l_m) \tag{1.6}$$

The neighborhood function is important because it helps to prevent islands of one structure in another at the structure edges, which would be incompatible with known anatomy (obviously, in rare cases of GM heterotopia some of the basic FreeSurfer assumptions would not be met) . Third, the probability distribution function (*PDF*) of the measured value is estimated separately for each label at each point. The PDF is modeled as a normal distribution, thus only the mean and variance for each label at each point have to be estimated.

The classification of each point in space to a given label for a test subject data set is achieved by finding the segmentation that maximizes the probability of the input given the prior probabilities from the training set. First, the probability of a class at each point is computed; it is the probability that the given class appeared at that point in the training set times the likelihood of getting the subject-specific measured value from that class (Fischl et al., 1999). The latter is computed from the PDF for that label as estimated from the training set. In this way, the probability of each class at each point is computed. An initial segmentation is generated by assigning each point to the class for which the probability is greatest. Given this segmentation, the neighborhood function is used to re-compute the class probabilities. The data set is iteratively re-segmented based on this new set of class probabilities. This is repeated until the segmentation converges. This procedure allows the atlas to be customized for each test subject by using the information specific to that data set.

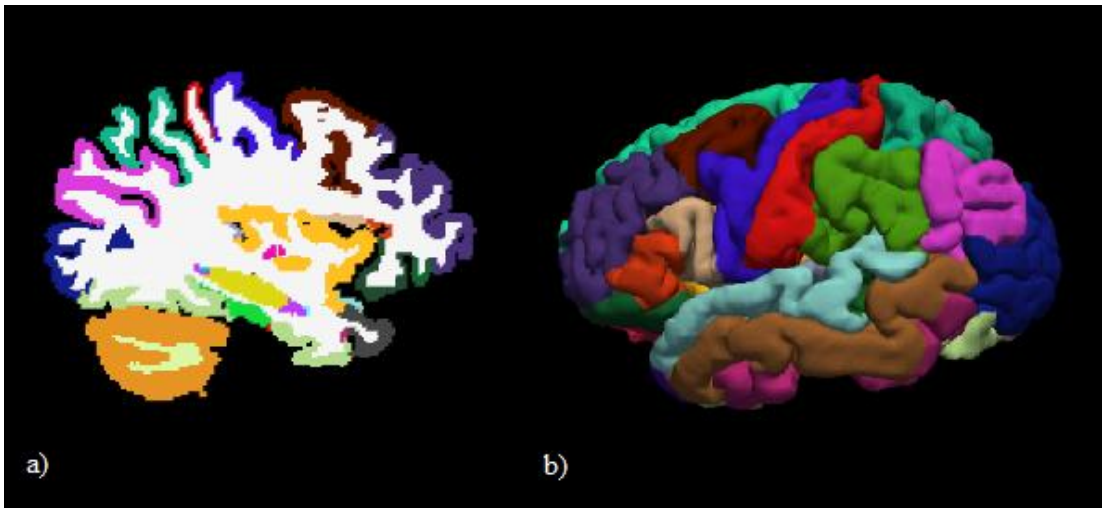

Figure 1.5 a) Volume-based and b) surface-based labeling. Among the others, it is easy to identify the precentral gyrus (electric blue) and the postcentral gyrus (red). These images are taken from a representative subject of the current study.

1.3 **Diffusion-weighted contrast: from DWI to DTI and TRACULA**

So far, we have discussed only the morphological reconstructions, and how to subdivide the cortex of a subject to obtain cortical measures. In the present study, cortical assessment of thickness and surface area were combined with DTI measures of connected and non-connected WM tracts. Therefore the next sections will discuss how TRACULA was used to reconstruct in vivo major WM tracts and obtain measures of WM integrity.

1.3.1 *DWI basic principles*

Diffusion is a physical process that involves fluid molecules, which follow Brownian motion. Specifically, water molecules moving in a solution without constraints, diffuse isotropically and their random motion is influenced only by their diffusion coefficient, namely by their molecular weight, intermolecular interaction (i.e., viscosity) and temperature (Beaulieu, 2002).

DWI takes advantage of this physical process in order to study tissue microstructure (Jones, 2008). The underlying cellular structure, indeed, affects the overall mobility of diffusing water by providing numerous barriers and by creating various compartments (e.g., intracellular and extracellular space, neurons, glial cells, axons, etc), which

hinder or constrain diffusion and define preferential directions for the motion (Beaulieu, 2002). In particular, since axons are highly straight structures, DWI is suitable for WM studies and for the assessment of micro-structural changes which statistically alter the displacement of water molecules per unit time (Jones, 2008). Hence, DWI allows an indirect observation of the water molecule diffusion by encoding this information in signal changes (Stejskal and Tanner, 1995). The diffusion weighting is obtained by means of an additional bipolar gradient pulse. If the phase of spins, which is voxel dependent, is set, and then diffusion occurs, water protons shuffling among neighboring voxels causes a loss of signal coherence and thus a reduction in signal amplitude (Figure 1.6). The echo time (TE) must be long enough to let diffusion be developed in a significant amount.

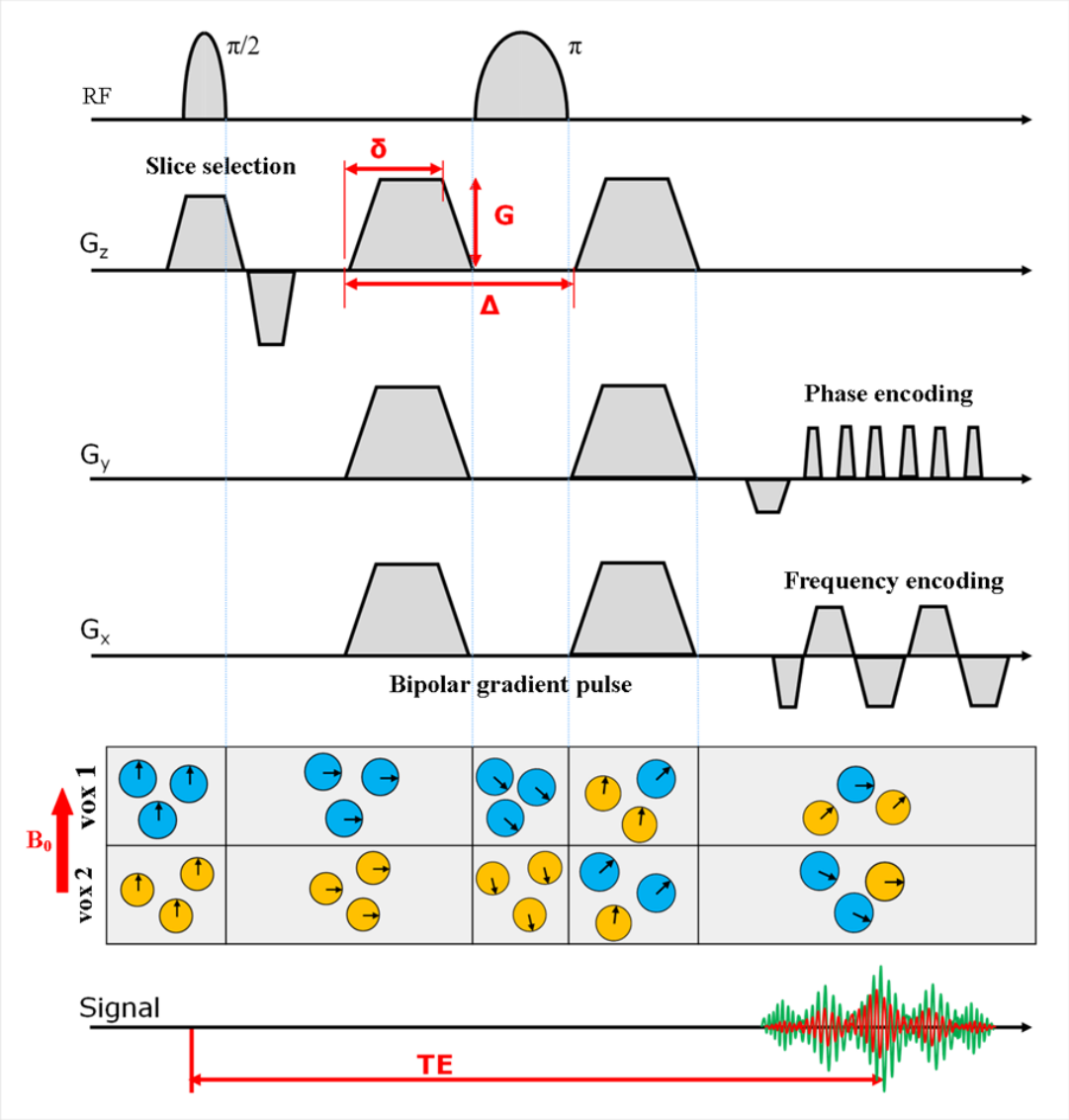

Figure 1.6 Diffusion weighted sequence by bipolar gradient pulse and EPI. If diffusion occurs, water molecules move to neighboring voxels and signal coherence is lost. In this case, recorded signal amplitude (in red) is lower than signal recorded when diffusion does not occur (superimposed in green).

Signal amplitude reduction is described by the following equation:

$$\frac{S}{S_0} = e^{-\gamma^2 g^2 \delta^2 \left(-\Delta \frac{\delta}{3}\right) ADC} = e^{-b\,ADC} \qquad (1.7)$$

where S is the diffusion weighted signal, S_0 is signal obtained when diffusion doesn't occur (T2-weighted image), δ is gradient pulse duration, G is the gradient pulse amplitude, Δ is the diffusion time, γ is the gyromagnetic ratio, while b [s/mm^2]

summarizes all the previous parameters and represents the diffusion sensibility level. The apparent diffusion coefficient (ADC [mm^2/s]) replaces the diffusivity coefficient D when describing the diffusion phenomenon within biological tissues, since it considers also the effect of water molecules interactions with cellular structures. Obviously, ADC < D. Generally, ADC is direction-dependent (Jones, 2008), hence anisotropic. In isotropic tissues, the water molecules move equally in all directions and ADC is a single constant. In anisotropic tissues, instead, ADC reflects tissue microstructure due to the diffusion directions. Therefore, in the voxels containing non-homogeneous biological microstructures, different signals are recorded for different gradient directions. Hence, it is important to acquire brain volumes using various bipolar gradient directions (six, at least, twelve in the case of this study) in order to obtain many ADC maps, either to extract directional information or to estimate the underlying mean diffusivity (MD) with no bias from the explored direction.

1.3.2 *DTI-based tractography*

It should be clear now that, when dealing with biological tissues with oriented structures like WM, we cannot describe water molecular behavior with a single ADC coefficient per voxel. Therefore, diffusion characterization requires a tensor in every voxel that describes the molecular mobility along each direction and correlation between these directions (Figure 1.7) (Le Bihan et al, 2001). Therefore DTI, an extension of traditional diffusion imaging, is used.

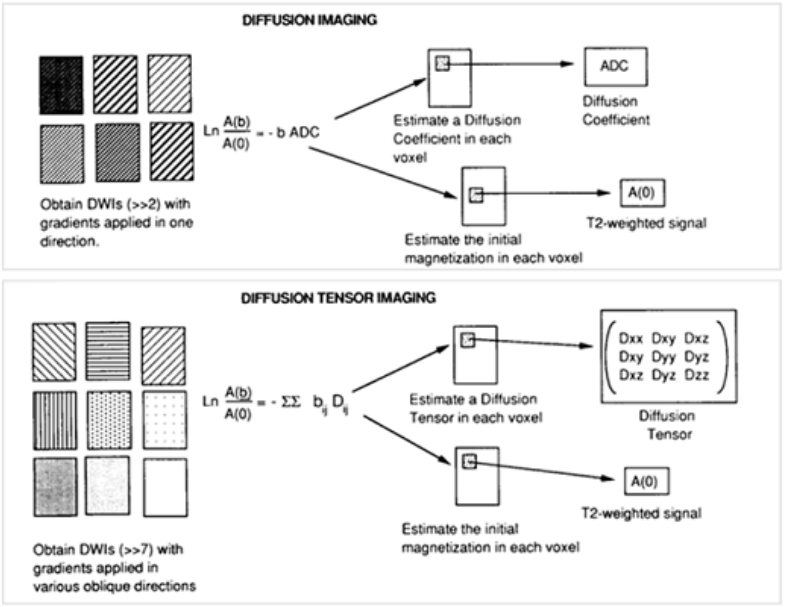

Figure 1.7 Diffusion imaging (upper panel) and diffusion tensor imaging (lower panel) (Le Bihan et al., 2001). Note how in DTI a diffusion tensor is estimated for each voxel instead of a diffusion coefficient (ADC)

The most useful application of DTI acquisition is tractography, which allows for the reconstruction of WM fiber bundle trajectories by piecing together discrete estimates (i.e., voxel-based) of the underlying continuous fiber orientation field (Jones, 2008). For each voxel a diffusion tensor is estimated: it is a 3×3 symmetric matrix which models the local diffusion as a 3D Gaussian distribution (Behrens et al, 2003). Displacement profile is thus represented by an ellipsoidal envelope (Figure 1.8), whose principal axes are given by the tensor eigenvectors (Jones, 2008). The longest axis stands for the primary eigenvector (whose magnitude is represented by the highest eigenvalue λ_1) and it is hypothesized to reflect diffusion parallel to the fibers, or axial diffusivity (AD); the two shorter axes represent the directions of the second and the third eigenvectors, whose magnitudes (i.e. the second λ_2 and the third λ_2 eigenvalues) are averaged to provide a measure of diffusivity perpendicular to the fibers, or radial diffusivity (RD).

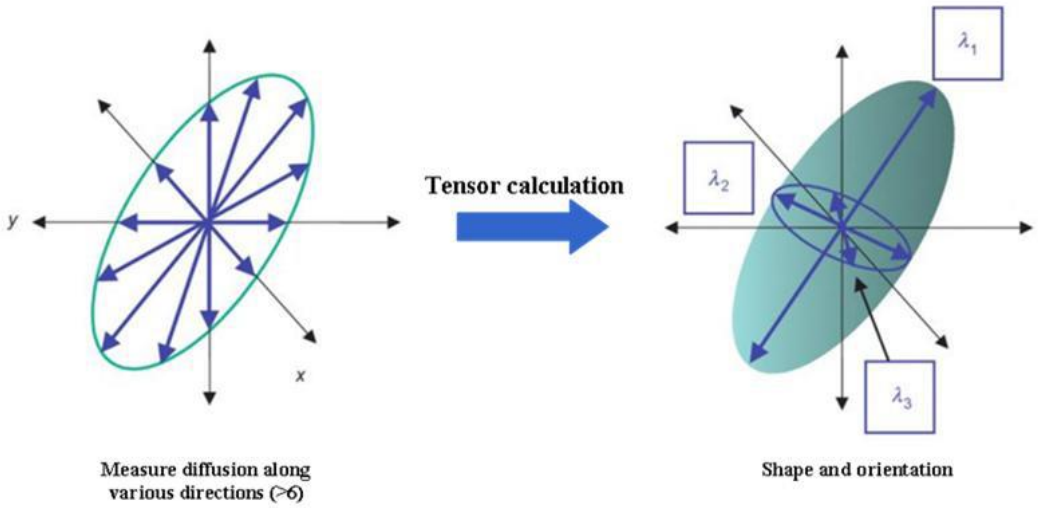

Figure 1.8 Elliptical representation of a diffusion tensor with the 3 main axes. (Sbardella et al., 2013) The longest axis stands for the primary eigenvector, whose eigenvalue (i.e. λ_1) reflects the diffusion parallel to the fibers; the two shorter axes represent the second (λ_2) and third (λ_3) eigenvectors, whose eigenvalues (i.e. λ_2 and λ_3) are averaged to provide a measure of diffusivity perpendicular to the fibers

The DTI metrics derived from a mathematical combination of all the three eigenvectors are mean diffusivity (MD),

$$\mathbf{MD} = \frac{\boldsymbol{\lambda}_1+\boldsymbol{\lambda}_2+\boldsymbol{\lambda}_3}{\mathbf{3}} \tag{1.8}$$

which measures overall water motion without any directionality, and fractional anisotropy (FA),

$$\mathbf{FA} = \sqrt{\frac{\mathbf{3}}{\mathbf{2}}\frac{(\boldsymbol{\lambda}_1-\mathbf{MD})^2+(\boldsymbol{\lambda}_2-\mathbf{MD})^2+(\boldsymbol{\lambda}_3-\mathbf{MD})^2}{\boldsymbol{\lambda}_1{}^2+\boldsymbol{\lambda}_2{}^2+\boldsymbol{\lambda}_3{}^2}} \tag{1.9}$$

which reflects the prevalence of diffusivity along one direction. MD is a quantitative metric of water diffusion; the higher the MD value, the higher the diffusivity. FA is a scalar value ranging from 0 to 1 that is highest in WM tracts, decreases in the GM, and approaches zero in the CSF.

Table 1.1 Schematic description of the main DTI parameters

	Unit of measure	Formula	Object measured
FA	Scalar value between 0-1	$\sqrt{\frac{3}{2}\frac{(\lambda_1 - MD)^2 + (\lambda_2 - MD)^2 + (\lambda_3 - MD)^2}{\lambda_1^2 + \lambda_2^2 + \lambda_3^2}}$	Fibers directionality
MD	mm^2/sec	$\frac{\lambda_1 + \lambda_2 + \lambda_3}{3}$	Amount of water diffusion
AD	mm^2/sec	λ_1	Diffusivity parallel to the fibers
RD	mm^2/sec	$\frac{\lambda_2 + \lambda_3}{2}$	Diffusivity perpendicular to the fibers

FA: fractional anisotropy; MD: mean diffusivity; AD: axial diffusivity; RD: radial diffusivity

According to the method used for voxel by voxel fiber reconstruction, tracking algorithms are defined as deterministic or probabilistic approaches.

In deterministic tractography the streamlines generation is sharply based on the direction of the local maximum eigenvector. The main assumption underlying the single-tensor deterministic tractography is that in each voxel the principal eigenvector is parallel to the dominant fiber orientation (Jones, 2008). Therefore, virtual fibers are reconstructed starting from a seed-point and extended forward in the next voxel following the principal direction. Stopping criteria are needed to reduce sensitivity to noise and partial volume effects: minimum FA threshold (usually 0.2) or maximum local curvature threshold are introduced (commonly 45° between nearest voxel) are introduced (Behrens er al., 2003). An example of DTI-based fiber tracking and associated stopping criteria is shown in figure 1.9

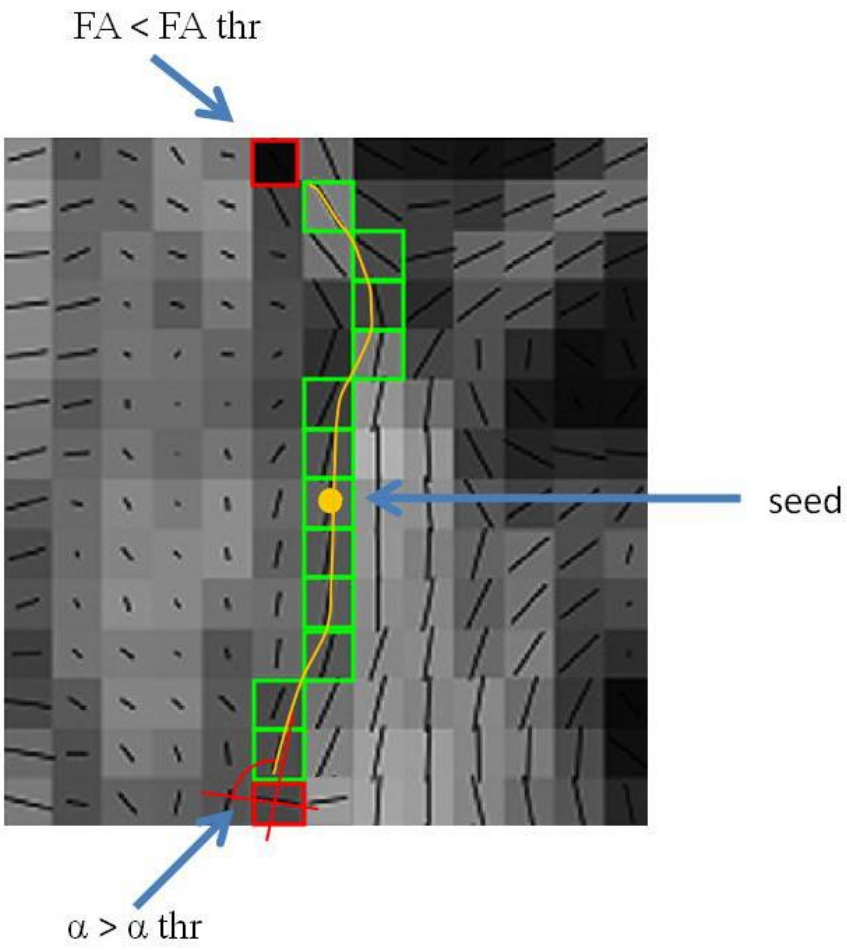

Figure 1.9 Stopping criteria in deterministic single tensor tractography. The image represents a FA map in gray scale from white (FA=1) to black (FA=0). In each voxel black lines represent the principal direction. The yellow spot represents the seed point, while the yellow line is the streamline tracked starting from the seed point. Green boxes highlight the path followed while red ones show the voxel where stopping criteria occur.

The main limitation of the single tensor imaging is the impossibility to recognize whether in a voxel branching, crossing or kissing fibers occurs (figure 1.10). This technique is unsuitable to describe fiber orientation when there is more than one fiber population within a voxel because each voxel is described by a single tensor (Jones, 2008). In these cases, since the tensor represent the average voxel structure, FA may decrease below threshold, thus interrupting both contingents of crossing fibers. In other cases, one tract can prevail, thus obscuring the other crossing one.

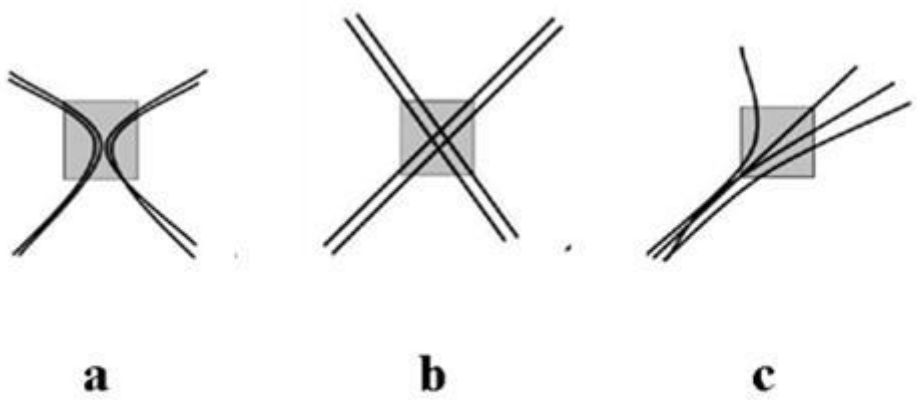

Figure 1.10 a) Kissing fibers; b) Crossing fibers; c) Branching fibers.

Another way to address the problem is adopting a completely different methodology using probabilistic algorithms.

1.3.3 *TRACULA*

Probabilistic tractography is a reconstruction technique that is based on partial volume model, as the *ball-and-stick* model. This model, as the name suggests, allows for multiple compartments of anisotropic diffusion (stick) and one compartment of isotropic diffusion (ball) per voxel (Behrens et al., 2007), and it is probabilistic since it fits in each voxel a distribution of fiber orientations instead of a single orientation.

TRACULA (TRActs Constrained by UnderLying Anatomy) is a method for automated reconstruction of major WM pathways that is based on the Bayesian probabilistic approach presented by Jbadbi et al. in 2007. However, it also utilizes prior information on the anatomy of the pathways from a set of training subject. This training dataset was obtained by manually labeling the WM pathways in each subject from the training cohort.

In the framework of Jbadbi et al. the unknown pathway *F* in any new test subject is estimated from the diffusion-weighted images *Y* of that subject via the posterior probability distribution of *F* given *Y*, as follow:

$$\boldsymbol{p}(\boldsymbol{F}|\boldsymbol{Y}) \propto \boldsymbol{p}(\boldsymbol{Y}|\boldsymbol{F})\boldsymbol{p}(\boldsymbol{F}) \tag{1.10}$$

where the likelihood *p(Y|F)* is the variability in the measured data given the shape of the pathway in the specific subject and the *a-priori* distribution *p(F)* as the variability in the pathway shape from subject to subject. (Yendiki et al., 2011) Therefore, the former is more linked to uncertainty due to measurement noise, while the latter to individual anatomical variation.

TRACULA uses the same formulation for the likelihood *p(Y|F)* as Jbadbi et al., which assumes Gaussian noise and uses the aforementioned *ball-and-stick* model of diffusion (Behrens et al., 2003). In particular, TRACULA uses *bedpostx* tool in FSL (http://fsl.fmrib.ox.ac.uk/) to estimate the distribution of the *ball-and-stick* model parameters at each voxel from the diffusion data, assuming up to two anisotropic compartments per voxel, besides the isotropic one. It should be noted that *bedpostx* does support the modeling of more than two fiber populations (i.e. anisotropic compartments) but TRACULA was specifically developed under the assumption of a maximum of two.

The main departure of TRACULA from the work by Jbadbi et al. is that, instead of assuming equal prior probability for all possible paths connecting two regions of interest, it uses an *a-priori* of the form:

$$\boldsymbol{p}(\boldsymbol{F}) = \boldsymbol{p}(\boldsymbol{F}\,|\boldsymbol{A}, \{\boldsymbol{F}_k\}_{\boldsymbol{k=1}}^{\boldsymbol{Nt}}, \{\boldsymbol{A}_k\}_{\boldsymbol{k=1}}^{\boldsymbol{Nt}}) \tag{1.11}$$

where A is the anatomical segmentation map of the cortical and subcortical non-WM structures of the test subject operated by FreeSurfer, F_k, k=1,…,N_t is the pathway of interest in each of the N_t training subjects, and A_k, k=1,…,N_t is the anatomical segmentation map of each training subject. In this way TRACULA uses the prior information on the anatomy of the pathway in the training subjects to increase the knowledge on the anatomy of the pathway in the test subject.

The process is divided in two steps: a first one operating on the training dataset to gain information about which anatomical regions the pathway intersects and about the neighbors along its trajectory, and a second one that applies this information to the test subject.

For each training subject, the anatomical segmentation map A_k, obtained from the T1 image using FreeSurfer, and the pathway F_k, obtained from the manual labeling of streamlines during training, are coregistered to the MNI space. The streamlines from

the manual labeling of the training subjects are divided into N_s segments along their trajectory with any segment extended along at least 3 voxels. Then seven histograms are computed for each segment i=1,…, N_s of each streamlines of the F_k pathway: one histogram counts how often each label a occurs in each voxel of the considered segment in the segmentation map A_k; the other six histograms do the same for its neighbor voxels that have in common one face (left, right, anterior, posterior, superior, and inferior). This yields the estimates of seven *a-priori* probability (the same probabilities is assigned to each voxel of the same segment): $p_i^0(a)$, that is the probability of being labeled a for a voxel in the i-th segment, and, similarly $p_i^L(a)$, $p_i^R(a)$, $p_i^A(a)$, $p_i^P(a)$, $p_i^I(a)$, $p_i^S(a)$ for its neighbors. These probabilities form a statistical framework for introducing into the tractography algorithm the same type of anatomical knowledge that an expert would use to label the pathways manually.

Once having concluded the first step of the process, the test subject is coregistered into MNI space to compute the prior probability $p(F\,|A,\{F_k\}_{k=1}^{Nt},\{A_k\}_{k=1}^{Nt})$ of a path, then the paths are divided into the same number of segments N_s of the corresponding training paths. Let the test path F go through N_v voxels in the common space; from the test subject's segmentation map A seven labels can be obtained for each of the j, j=1,…, N_v voxels: a_j^0, a_j^L, a_j^R, a_j^A, a_j^P, a_j^I, a_j^S. The prior probability of the considered path is assumed to be the product of the prior probabilities of each voxel along the path:

$$\boldsymbol{p(F\,|A,\{F_k\}_{k=1}^{Nt},\{A_k\}_{k=1}^{Nt}) =}$$
$$\boldsymbol{\prod_{j=1}^{Nv} p_{i(j)}^0(a_j^0)\, p_{i(j)}^L(a_j^0)\, p_{i(j)}^R(a_j^R)\, p_{i(j)}^A(a_j^A) p_{i(j)}^P(a_j^P)\, p_{i(j)}^I(a_j^I)\, p_{i(j)}^S(a_j^S)} \quad (1.12)$$

Where *i(j)* highlights that the *j*-th voxel belongs to the *i*-th segment.
Then the posterior distribution *p(F|Y)* for the path *F* of the test subject is estimated via a Markov Chain Monte Carlo (MCMC) algorithm. This final step of the process (Yendiki et al. 2011) is not detailed here, but it is worth to remark that the training dataset, in addition to the estimation of the anatomical priors, is also used to derive the initialization of the MCMC algorithm and to constrain the perturbations in each iterative step of the latter.

It should be noted that TRACULA provides a key benefit over traditional tractographic algorithms. Specifically, the focal WM pathology common to MS

patients often prevents the successful reconstruction of fiber bundles. Deterministic algorithms often terminate when reaching the decreased FA of a lesion. The common solution of surrogating individual DTI information with atlas topology, though effective loses subject specific details. Probabilistic algorithms generally perform better in this regard with respect to deterministic ones. However, depending on the severity of the tissue destruction, they are not necessarily sufficient. Thus, in the context of the current study, the anatomical priors utilized by TRACULA provide an additional means to overcome some of the inherent difficulties presented by MS WM lesions. In summary, this approach appears to exploit all pros of atlas based analyses, utilizing them not as absolute references but as priors, and individual probabilistic reconstructions.

1.4 **Conclusion**

In conclusion, the present introductory chapter has presented both some theoretical aspects and the practical features of up-to-date algorithms to be employed in this thesis work. This in order to achieve a combined study of the relationship between WM tracts and connected cortical GM regions. In particular using FreeSurfer to gather data about the parcellation of the cortex and TRACULA to glean data about the DTI measures of six WM tracts.

2. MATERIALS AND METHODS

2.1 **Subjects**

This study included thirty-two patients with relapsing-remitting multiple sclerosis (RRMS). At the time of MRI acquisition, MS patients were in a relapsing phase and steroid-free since three months, at least. RRMS patients with any other pre-existing medical condition were also excluded.

Thirty healthy controls (HC) were recruited from volunteers who had a normal neurological examination with no history of neurological, psychiatric, cardiovascular or metabolic disorders.

All study participants provided written informed consent. The study was approved by the 'Don Carlo Gnocchi Foundation' ethics committee, Milan, Italy.

2.2 **MRI acquisition**

All scans were acquired on the same 1.5T MRI scanner (Siemens Magnetom Avanto, Erlangen, Germany) by a 12-channel head matrix coil.

Figure 2.1: Siemens Magnetom Avanto, Erlangen, Germany

Three sequences were acquired: 1) dual-echo turbo spin echo proton density (PD)/T2-weighted (*repetition time (TR)=2650ms; echo time (TE)=28/113ms; echo train length = 5; 50 contiguous 2.5-mm thick axial slices; 1mm^2 in-plane resolution*); 2) three-dimensional T1-weighted Magnetization-Prepared RApid Gradient Echo (MP-RAGE) (*repetition time (TR)=1900ms; echo time (TE)=3.37ms; inversion time (TI)=1100ms; flip angle α=15°; 176 contiguous 1-mm thick axial slices; 1mm^2 in-plane resolution)*; 3) diffusion weighted (DW) pulsed-gradient spin echo planar (*repetition time (TR)=7000ms; echo time (TE)=94ms; 50 contiguous 2.5-mm thick axial slices; 2mm^2 in-plane resolution; diffusion gradients applied in 12n non-collinear directions with a b-value=900 s/mm^2; number of runs=2).* A brief review of the parameters used can be found in the following tables.

Table 2.1 Dual-echo turbo spin echo Proton Density (PD)/T2-weighted

	TR [ms]	**TE [ms]**	**Train Lenght**	**slices**	**Resolution [mm^3]**
PD/T2	2650	28/113	5	50	1x1x2.5

Table 2.2 Three-dimensional T1-weighted Magnetization-Prepared RApid Gradient Echo (MP-RAGE)

	TR [ms]	**TE [ms]**	**TI**	**α [°]**	**slices**	**Resolution [mm^3]**
MP-RAGE	1900	3.37	1100	15	176	1x1x1

Table 2.3 Diffusion Weighted (DW) pulsed-gradient spin echo planar

	TR [ms]	**TE [ms]**	**directions**	**b-value [s/mm^2]**	**slices**	**Resolution [mm^3]**
DWI	7000	94	12	900	50	2x2x2.5

Among the three sequences the first two addressed anatomical features: PD/T2 to measure WM lesion volume, whereas MP-RAGE for high-resolution brain morphology, and measures of cortical thickness and areas. The third sequence, DW,

which exploits the diffusion of water in the brain, was used for the assessment of tissue microstructure integrity and WM tract reconstruction, as better explained in 1.3.

2.3 **Lesion segmentation**

Among the acquired sequences, the PD/T2-weighted scans were used for WM lesions segmentation in the acquisitions of the thirty-two MS patients. In particular, segmentation was performed using the PD-weighted images of PD/T2 scans, while the T2-weighted images were used to validate the former segmentation.

This process was performed by an experienced neurologist on the JIM software (http://www.xinapse.com) version 5, which utilizes a semi-automated, local thresholding technique.

The identified lesions were used for the pre-processing of the T1-weighted images in order to prevent confounds in WM/GM segmentation. In fact, WM are hypointense in T1 contrast and can be misclassified with GM by automated segmentation techniques. It has been shown that such misclassifications can significantly affect both tissue volumetry (Battaglini et al., 2012) and cortical thickness (Magon et al., 2014) measurements. To reduce the impact of T1 hypointensities, lesion filling, by in-painting the average WM intensity, is recommended as preprocessing step. In the current work, *lesion_filling* tool (Gelineau-Morel et al., 2012), part of FMRIB's Software Library (FSL), was used.

2.4 **Tract-cortex correspondences**

This work aims at studying the correlation between GM and WM in thirty-two MS patients and comparing the results with the same analysis performed on thirty healthy controls.

Thus, a major step was to a-priori define which cortical region had to be correlated with each tract.

For this purpose approaches from an attentive analysis of previous works (Catani et al., 2012, Wakana et al., 2004, Catani et al., 2001, Burgel et al. 2005, Thiebaut de Schotten et al., 2010, Lawes et al., 2007, Felten et al., 2004, FitzGerald et al., 2002) were implemented in an "in-house" application, consisting in visualizing the

reconstructed tracts on the parcellation of the cortex and evaluating which gyri were more "involved" by the endings of each tract (Figure 2.2). Refer to next two paragraphs for details.

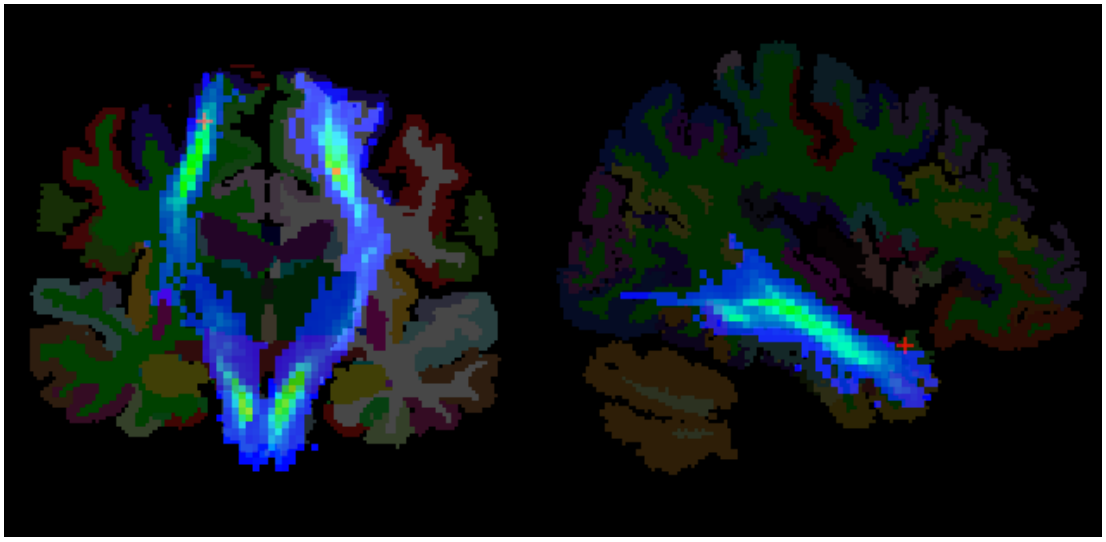

Figure 2.2 Corticospinal tract (CST, left) and inferior longitudinal fasciculus (ILF, right) probability maps visualized, in coronal and sagittal view respectively, on the parcellation of the cortex. Warmer colors indicate higher probability of corresponding to the tract of interest. Colors on the anatomical image correspond to automatically parcellated labels from FreeSurfer.

Good correspondences were found between literature and our method. The chosen cortical region and the relative WM tracts are listed in 2.5 and 2.6, respectively

2.5 **Morphological reconstruction**

3D T1 sequence (figure 2.3), lesion filled for the MS patients, were used as input to FreeSurfer processing stream version 5.3, which operates a morphological reconstruction of the brain, through the tool *recon_all*.

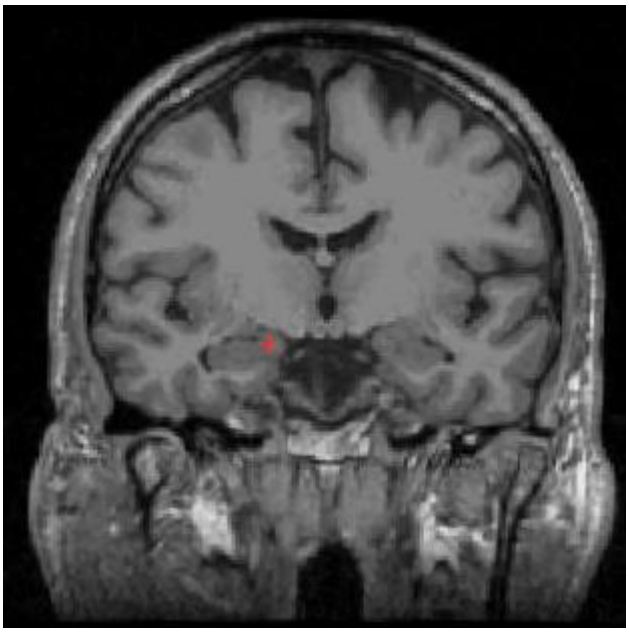

Figure 2.3 Example of coronal view of a 3D T1 image

As explained in 1.2 the main output of this process was the segmentation of cortex GM and sub-cortical brain (WM and deep GM structures, though referred to as WM mask, in brief). Importantly, the vector description of the cortex addresses a subject-independent common topology, thus permitting the parcellation in sub-regions of the cortex. A WM mask example is shown in figure 2.4, in which a further segmentation subcortical GM was performed by exploiting the intensity gradient in the image, to localize the GM/WM boundary surfaces.

The extracted WM surface was then made grow to obtain the pial surface, between the GM and sulcal cerebrospinal fluid (CSF).

Once reconstructed, the cortex, thus the region comprises between the pial and the gray/WM surfaces, it was parceled according to the DKT40 atlas in different anatomical areas. Measures of cortical thickness were next obtained as the average of the distances calculated at each vertex between the pial and the GM/WM surfaces (Figure 2.5).

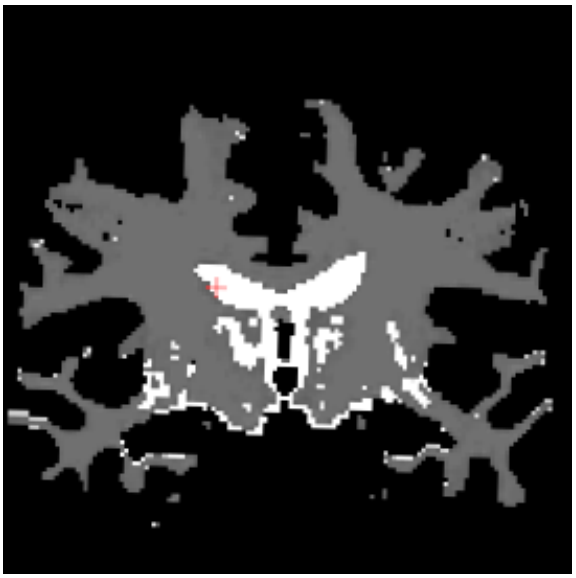

Figure 2.4 White matter mask

Among all the DKT40 atlas regions, the following ones were selected to extract thickness and surface area measures:

- Caudal and rostral middle frontal gyri
- Latero-orbital gyrus
- Superior frontal gyrus
- Precentral gyrus
- Supramarginal and superior parietal gyri
- Lateral occipital gyrus
- Middle and inferior temporal gyrus
- Superior temporal gyrus

Note that the terms “area”, “region” and “gyrus” are always used as synonymous between each other in the present work.

In the above list, some adjacent regions, are paired. In these cases, the correlation of cortical features with DTI measures of tracts was assessed both for the separate regions and for the pairs, thus considering the average of cortical features. In doing this, the influence of one tract was hypothesized to be equivalent on the two regions.

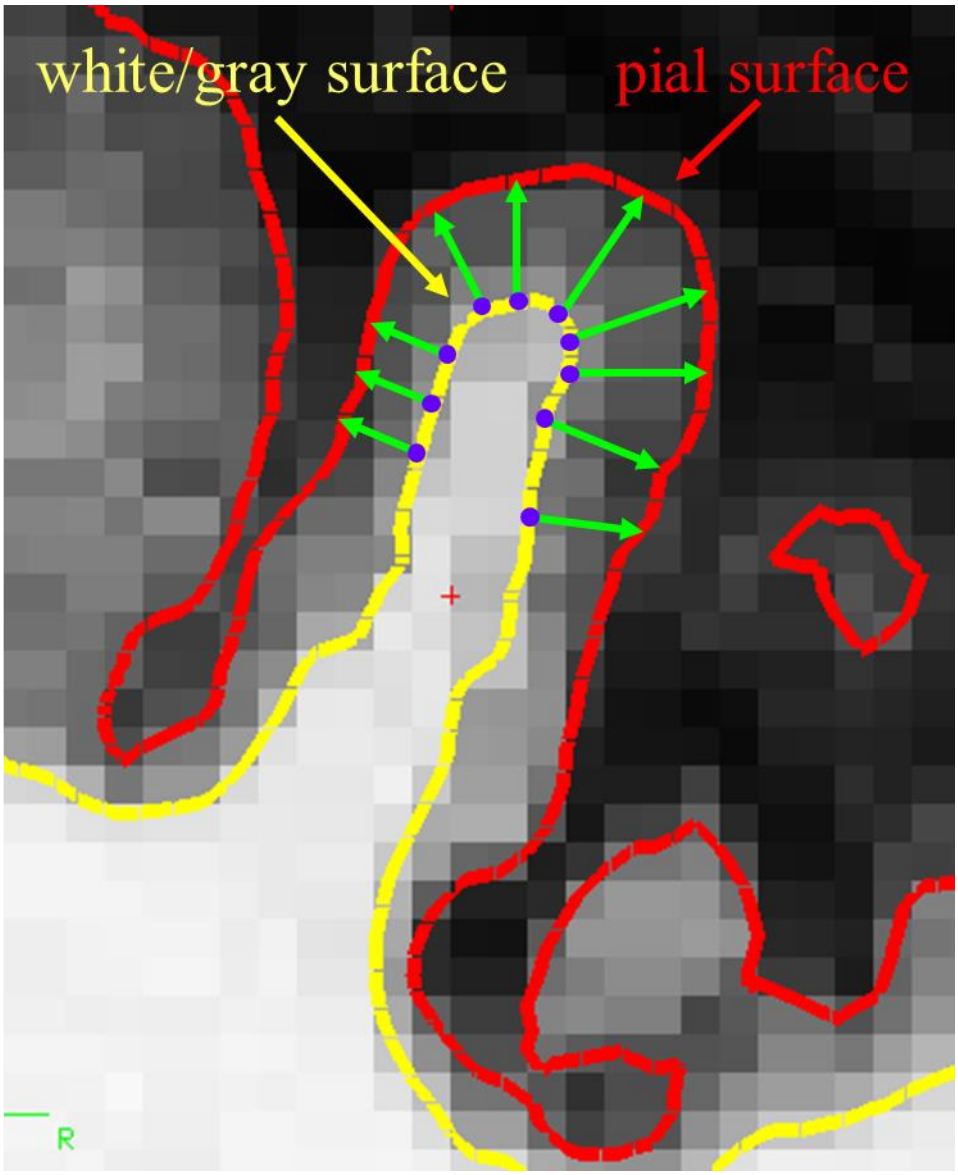

Figure 2.5 Image of a gyrus of the brain with highlighted the pial surface (red) and the white/gray matter surface (yellow). Cortical thickness calculated as the distance at each vertex of the mash between pial and white/grey matter (yellow) surfaces.

The measures of both cortical thickness and surface area for the left and the right hemispheres were obtained separately, but further calculations were done.

In fact, the thickness of a region of the cortex was calculated as the average of the thicknesses, weighted by the surface area of that region in the two different hemispheres, as follow:

$$\boldsymbol{thickness} = \frac{\boldsymbol{thickness}_{\text{left}} \times \boldsymbol{area}_{\text{left}} + \boldsymbol{thickness}_{\text{right}} \times \boldsymbol{area}_{\text{right}}}{\boldsymbol{area}_{\text{left}} + \boldsymbol{area}_{\text{right}}} \qquad (2.1)$$

While the surface area of a region was calculated as the sum of the surface areas of that region in the two hemispheres, as follow:

$$\boldsymbol{area} = \boldsymbol{area}_{\text{left}} + \boldsymbol{area}_{\text{right}} \qquad (2.1)$$

The total intracranial volume of each subject (TIV) was also obtained, based on the determinant of the Talairach registration (see section 1.2 describing the reconstruction stream).

2.6 **Reconstruction of the tracts**

Once gathered data about the morphology of the cortical regions listed above, we worked on the Diffusion weighted images (DWI) using another FreeSurfer tool: TRACULA (TRActography Constrained by the UnderLying Anatomy).

As depicted in 1.3.3, TRACULA is a tool for the automatic reconstruction of a set of fascicles, based on global probabilistic tractography and anatomical priors. This is the reason why we input to TRACULA, for each subject, not only the raw data of the diffusion weighted scans, but also the morphological reconstructions of the cortex, previously operated with the tool *recon-all* of FreeSurfer.

In this way, we obtained the measures of axial, radial and mean diffusivity (AD, RD, MD) and fractional anisotropy (FA) of a set of WM tracts. TRACULA gives as output three "versions" of the four indexes for each reconstructed tract:

1) average over the entire support of the path distribution

$$\boldsymbol{FA}_{\text{avg}} = \frac{\sum_{\boldsymbol{i}=\boldsymbol{1}}^{\boldsymbol{N}} \boldsymbol{FAi}}{\boldsymbol{N}} \qquad (2.3)$$

where FA can be substituted with one among AD, RD or MD;
2) weighted average over the entire support of the path distribution

$$\boldsymbol{FA}_{\text{avg\_weight}} = \frac{\sum_{\boldsymbol{i=!}}^{\boldsymbol{N}} \boldsymbol{p}_{\text{i}} \cdot \boldsymbol{FA}_{\text{i}}}{\sum_{\boldsymbol{i=1}}^{\boldsymbol{N}} \boldsymbol{p}_{\text{i}}} \tag{2.4}$$

where p is the probability of every streamlines to belong to the correspondent tract;
3) average over the highest-probability path only

$$FA_{\text{avg\_center}} = \arg\max_{\text{FA}} \{p\} \tag{2.5}$$

where p is the probability of each streamlines to belong to the correspondent tract.

We decided to use only the probability weighted average of the four indexes, as indicated in 2.4, as long as this measure was thought to be the one among the three to have better properties of generality and accuracy, thanks to the weighing by the probabilities.

The DTI measures were obtained separately for the left and right tracts, but, as well as for the cortical measures, averages weighted on the volume of the respective tract were calculated to be used for further analysis, as follow:

$$FA = \frac{\boldsymbol{FA}_{\text{left}} \times \boldsymbol{volume}_{\text{left}} + \boldsymbol{FA}_{\text{right}} \times \boldsymbol{volume}_{\text{right}}}{\boldsymbol{volume}_{\text{left}} + \boldsymbol{volume}_{\text{right}}} \tag{2.6}$$

Among the reconstructed tracts, we focused only on those that previous studies demonstrate to contribute to the major cognitive circuits, as previously discussed in the introduction, and to functionally and anatomically connect the different regions of the cortex, listed in paragraph 2.5:

- Anterior thalamic radiation (ATR) from thalamus to the caudal-rostral middle frontal gyri
- Corticospinal tract (CST) from brainstem to the precentral gyrus
- Inferior longitudinal fasciculus (ILF) from the lateral occipital gyrus to the the middle temporal and the inferior temporal gyri
- Superior longitudinal fasciculus – parietal endings (SLFP) from the superior frontal gyrus to the supramarginal and the superior parietal gyri

- Superior longitudinal fasciculus – temporal endings (SLFT) from the superior frontal gyrus to the superior temporal gyrus
- Uncinate (UNC) from the lateral orbito-frontal gyrus to the middle temporal and the inferior temporal gyri

TRACULA also reconstructs the cingulum and the forceps major and minor of the corpus callosum, but, for our work, those tracts were excluded. In particular, the cingulum was excluded because it is characterized by fan-like endings towards a very large number of different gyri, thus it would not be informative to correlate its integrity measures with the cortical morphology of areas spread almost all over the brain. While the two parts of the corpus callosum were excluded because their activity of connection of hemispheres is not in the focus of our work and also because it is not easy to correlate the activity of the corpus callosum with any specific region of the cortex.

2.7 **Statistical analysis**

Once gathered the data about the WM tracts and the associated cortical areas, we proceeded with the statistical analysis, performed using SPSS (version 16; IBM Corp., Armonk, NY, USA).

2.7.1 *Demographic characteristics*

First, the demographical characteristics of the cohort were studied. In particular, demographic differences between MS patients and healthy controls were tested using Student's *t*-test and Fisher's exact test for age and sex, respectively; *p*-values<0.05 indicated significant differences using two-tailed tests.

2.7.2 *Normality test*

The Normality of the distribution of the variables, within each group, was assessed both using the Kolmogorov-Smirnov test and through the analysis of the histograms.

2.7.3 *ANCOVA*

Group differences between cortical thickness, surface area and DTI measures were assessed using an ANCOVA model, with the worthwhile visual help of boxplots. Age and sex were used as covariates for cortical thickness and DTI measures, while, for surface area measures, total intracranial volume (TIV) was also included as a covariate.

2.7.4 *Partial correlation*

The same covariates were used to analyze the partial correlations between the index of tracts integrity and the measures of the regions of the cortex that these tracts connect with each other, as listed in 2.6.

Thus, FA, AD, RD and MD of ILF were correlated with the cortical measures (thickness and area) of, by one side, lateral-occipital gyrus and, by the other side, middle temporal and inferior temporal gyri. Whereas a tract impinges onto two adjacent gyri of the same lobe, as in this case for the middle and the inferior gyri of the temporal lobe, the correlation of the DTI index were also correlated with the average of the cortical measures.

The same was done for the other considered tracts and the gyri they impinge on. Thus SLFP measures were correlated with, by one side, superior frontal gyrus and, by the other side, supramarginal gyrus, superior parietal gyrus and their average measures; SLFT, by one side, with superior frontal gyrus and, by the other side, superior temporal gyrus; UNC with, by one side, latero-orbital gyrus, and, by the other side, inferior temporal, middle temporal gyri and their average measures. ATR was correlated with the caudal-middle frontal, the rostral-middle frontal gyri and also their average measures, while CST was correlated with the precentral gyrus. It is to be noted that the latter two tracts were correlated with the cortical morphology of regions from only one lobe, as long as, they are not associative fibers but projective ones, in fact ATR and CST connect the thalamus and the brainstem, respectively, to the cortex.

Although MS causes widespread damage throughout the brain, we expected stronger relationships with anatomically connected tracts than for those that are not, and one of the main aim of this work is to test this hypothesis. Thus, each tract was correlated for comparison with a region chosen among those the tract is not connected to. ILF was correlated with the precentral gyrus, UNC was correlated with the average

of the supramarginal and the superior temporal giry while ATR, CST, SLFP and SLFT were correlated with the lateral occipital gyrus.

2.7.5 *Multiple Linear Regression*

In order to analyze whether the contribution of one or more connected tract were higher than the contribution of a not-connected tract in predicting the thickness of a certain region of the cortex for RRMS patients, a multiple linear regression (MLR) analysis was performed.

Thus, for each lobe, the thickness of a gyrus was chosen as predicted variable (output), while the DTI indexes of both the related tract and a non related tract were considered as predictors; the latter being given the role of separating confounds due to generalized damage. The considered combinations were as follow:

- Outcome: middle temporal and inferior temporal average thickness
  Predictors: UNC and ILF (proximal) vs SLFP (distal) DTI measures
- Outcome: supramarginal and superior parietal average thickness
  Predictors: SLFP (proximal) vs UNC (distal) DTI measures
- Outcome: superior frontal thickness
  Predictors: SLFP and SLFT (proximal) vs CST (distal)
- Outcome: lateral occipital thickness
  Predictors: ILF (proximal) vs UNC (distal)

Covariates, (age and sex) were input into the first block of the model (enter method), then, MRI measures in the second (forward-stepwise method).

3. RESULTS

3.1 **Healthy controls and patients comparison**

Thirty healthy controls and thirty-two RRMS patients were enrolled in this study, which has the aim of analyzing the relationship between WM tracts and both connected and non-connected regions of cortical GM.

3.1.1 *Demographic characteristics*

First, the demographic characteristics of the cohort were studied. In particular, demographic differences between MS patients and healthy controls were tested using Student's *t*-test and Fisher's exact test for age and sex, respectively; *p*-values < 0.05 indicated significant differences using two-tailed tests.

Table 3.1 provides an overview of the demographic characteristics of the cohort. No significant demographic differences between the two groups were found.

Table 3.1 Demographic characteristics of healthy controls and relapsing-remitting multiple sclerosis patients.

	RRMS (*N = 32*)	**HC (*N = 30*)**	***p***
Age in years, mean (SD)	41.28 (10.66)	38,17 (12,75)	**0.3**
Sex, female, N (%)	18 (56,2)	17 (56,7)	**1.0**

Demographic differences were tested using Student's *t*-test and Fisher's exact test for age and sex, respectively.
HC: healthy controls; RRMS: relapsing-remitting multiple sclerosis; *N*: number; SD: standard deviation

Figure 3.1 shows the boxplots of the age for the two groups. Only the age (70) of one RRMS patients was identified as an outlier, bringing to a higher average of the age of the patients with respect to the healthy controls, but without being significantly different ($p = 0.3$). The subject was included in further analysis.

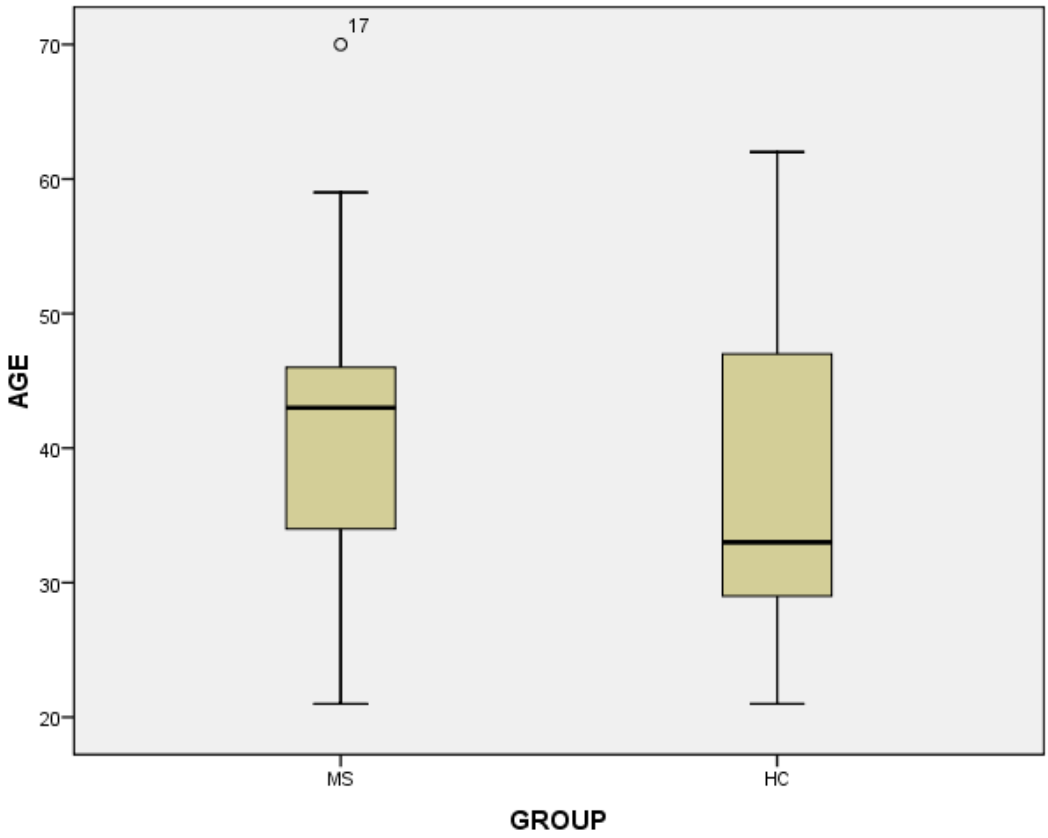

Figure 3.1 Boxplots (also called *box and whisker* diagram) of the age for the two groups. The distance between the lowest horizontal line and the lowest edge of the tinted box is the range between which the lowest 25% of scores fall (*bottom quartile*), the tinted box shows the *interquartile range*, while the distance between the top edge and the top horizontal line represents the *top quartile.* The ticker horizontal line shows the value of the median, while the circles are cases deemed to be outliers.

3.1.2 *ANCOVA for MRI characteristics*

3.1.2.1 Tracts measures

Group differences between tracts DTI measures were assessed using an ANalysis of COVAriance (ANCOVA) model, with the worthwhile visual help of boxplots. With respect to healthy controls, the WM tracts of RRMS patients were generally characterized by increased AD, MD and RD and decreased FA, as expected for the intrinsic characteristics of the disease, like axonal damage and loss of myelin.

3.1.2.1.1 Anterior thalamic radiations

Table 3.2 shows group differences between AD, RD, MD and FA for ATR. RRMS presented with significantly higher AD and MD.

Figure 3.2 shows boxplots of AD, RD, MD and FA for the two groups.

Table 3.2 Anterior thalamic radiations measures in healthy controls and relapsing-remitting multiple sclerosis

	RRMS (*N = 32*)	**HC (*N = 30*)**	***p***
	ATR measures		
AD	1.15 (0.03)	1.12 (0.02)	**0.003**
RD	0.58 (0.04)	0.56 (0.02)	0.153
MD	0.77 (0.03)	0.75 (0.02)	**0.026**
FA	0.42 (0.03)	0.42 (0.02)	0.784

HC: healthy controls; RRMS: relapsing-remitting multiple sclerosis; N: number; ATR: anterior thalamic radiations
Data are presented as mean (standard deviation). AD, RD and MD are given in $mm^2/s * 10^{-3}$. FA is a dimensionless index.
p-values were calculated using ANCOVA, controlling for age and sex. Significant differences are shown in bold

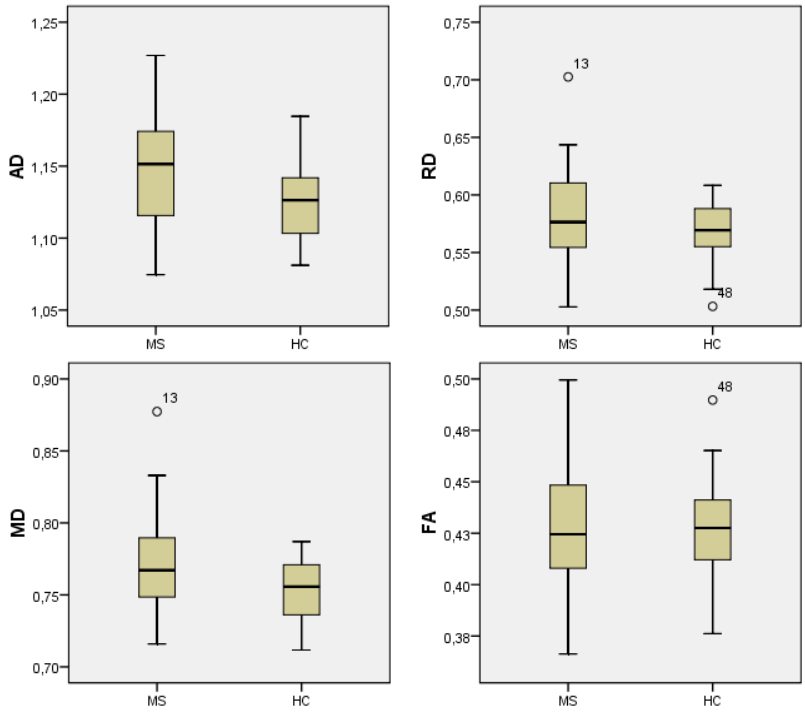

Figure 3.2 Boxplots of AD, RD, MD and FA of ATR for relapsing-remitting multiple sclerosis and healthy controls

3.1.2.1.2 Corticospinal tract

Table 3.3 shows group differences between AD, RD, MD and FA for CST. RRMS presented with significantly higher AD, RD and MD.

Figure 3.3 shows boxplots of AD, RD, MD and FA for the two groups.

Table 3.3 Corticospinal tract measures in healthy controls and relapsing-remitting multiple sclerosis

	RRMS (*N = 32*)	**HC (*N = 30*)**	***p***
	CST measures		
AD	1.19 (0.03)	1.18 (0.02)	**0.046**
RD	0.54 (0.02)	0.53 (0.02)	**0.017**
MD	0.76 (0.03)	0.74 (0.02)	**0.007**
FA	0.49 (0.03)	0.48 (0.02)	0.190

HC: healthy controls; RRMS: relapsing-remitting multiple sclerosis; N: number; CST: corticospinal tract
Data are presented as mean (standard deviation). AD, RD and MD are given in $mm^2/s * 10^{-3}$. FA is a dimensionless index.
p-values were calculated using ANCOVA, controlling for age and sex. Significant differences are shown in bold

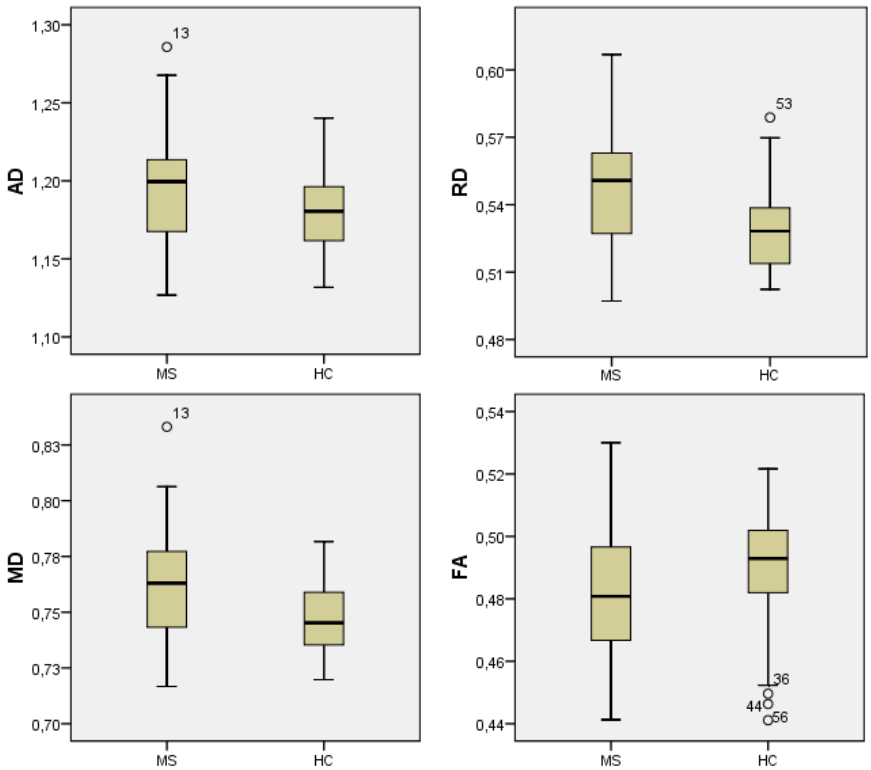

Figure 3.3 Boxplots of AD, RD, MD and FA of CST for relapsing-remitting multiple sclerosis and healthy controls

3.1.2.1.3 Inferior longitudinal fasciculus

Table 3.4 shows group differences between AD, RD, MD and FA for ILF. RRMS presented with significantly higher RD, MD and lower FA.

Figure 3.4 shows boxplots of AD, RD, MD and FA for the two groups.

Table 3.4 Inferior longitudinal fasciculus measures in healthy controls and relapsing-remitting multiple sclerosis

	RRMS (*N = 32*)	**HC (*N = 30*)**	***p***
	ILF measures		
AD	1.25 (0.05)	1.23 (0.05)	0.066
RD	0.66 (0.05)	0.59 (0.03)	**<0.001**
MD	0.85 (0.05)	0.80 (0.05)	**<0.001**
FA	0.40 (0.03)	0.45 (0.03)	**<0.001**

HC: healthy controls; RRMS: relapsing-remitting multiple sclerosis; N: number; ILF: inferior longitudinal fasciculus
Data are presented as mean (standard deviation). AD, RD and MD are given in $mm^2/s * 10^{-3}$. FA is a dimensionless index.
p-values were calculated using ANCOVA, controlling for age and sex. Significant differences are shown in bold

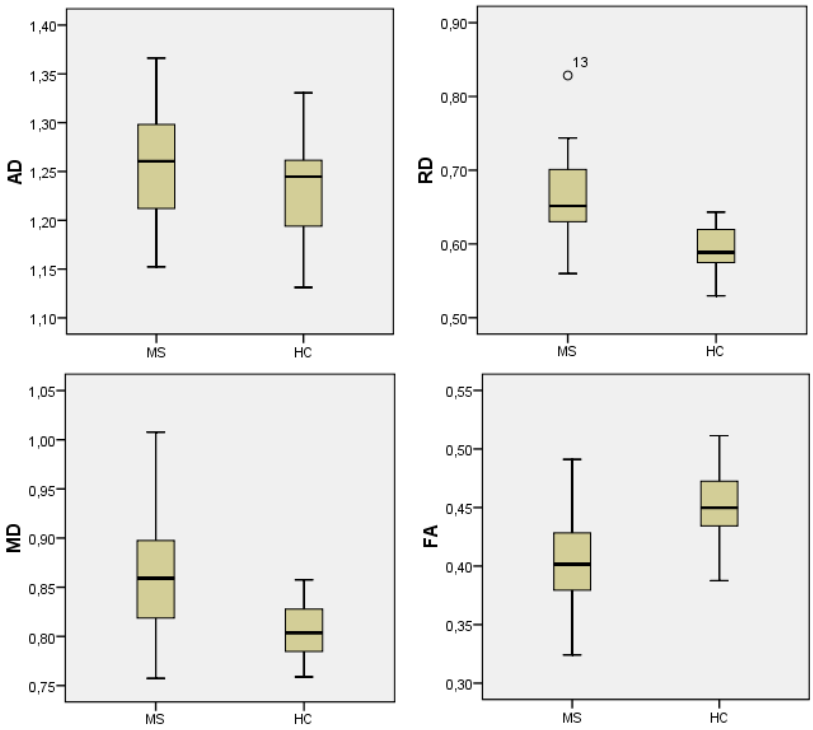

Figure 3.4 Boxplots of AD, RD, MD and FA of ILF for relapsing-remitting multiple sclerosis and healthy controls

3.1.2.1.4 Superior longitudinal fasciculus – parietal endings

Table 3.5 shows group differences between AD, RD, MD and FA for SLFP. RRMS presented with significantly higher AD, RD and MD.

Figure 3.5 shows boxplots of AD, RD, MD and FA for the two groups.

Table 3.5 Superior longitudinal fasciculus (parietal endings) measures in healthy controls and relapsing-remitting multiple sclerosis

	RRMS (*N = 32*)	**HC (*N = 30*)**	***p***
	SLFP measures		
AD	1.10 (0.05)	1.07 (0.02)	**0.004**
RD	0.59 (0.05)	0.57 (0.02)	**0.035**
MD	0.76 (0.04)	0.74 (0.02)	**0.012**
FA	0.40 (0.02)	0.41 (0.02)	0.614

HC: healthy controls; RRMS: relapsing-remitting multiple sclerosis; N: number; SLFP: superior longitudinal fasciculus – parietal endings
Data are presented as mean (standard deviation). AD, RD and MD are given in $mm^2/s * 10^{-3}$. FA is a dimensionless index.
p-values were calculated using ANCOVA, controlling for age and sex. Significant differences are shown in bold

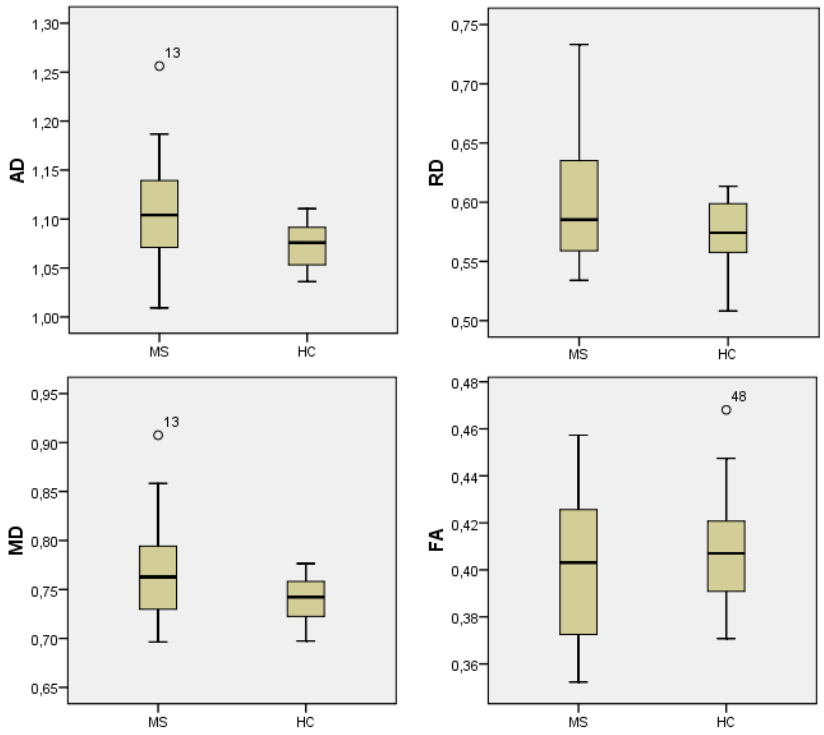

Figure 3.5 Boxplots of AD, RD, MD and FA of SLFP for relapsing-remitting multiple sclerosis and healthy controls

3.1.2.1.5 Superior longitudinal fasciculus – temporal endings

Table 3.5 shows group differences between AD, RD, MD and FA for SLFT. RRMS presented with significantly higher AD, RD, MD and lower FA.

Figure 3.5 shows boxplots of AD, RD, MD and FA for the two groups.

Table 3.6 Superior longitudinal fasciculus (temporal endings) measures in healthy controls and relapsing-remitting multiple sclerosis

	RRMS (*N = 32*)	**HC (*N = 30*)**	***p***
	SLFT measures		
AD	1.14 (0.05)	1.12 (0.02)	**0.033**
RD	0.61 (0.05)	0.57 (0.02)	**0.004**
MD	0.79 (0.05)	0.76 (0.02)	**0.006**
FA	0.40 (0.02)	0.42 (0.02)	**0.009**

HC: healthy controls; RRMS: relapsing-remitting multiple sclerosis; N: number; SLFT: superior longitudinal fasciculus – temporal endings
Data are presented as mean (standard deviation). AD, RD and MD are given in $mm^2/s * 10^{-3}$. FA is a dimensionless index.
p-values were calculated using ANCOVA, controlling for age and sex. Significant differences are shown in bold

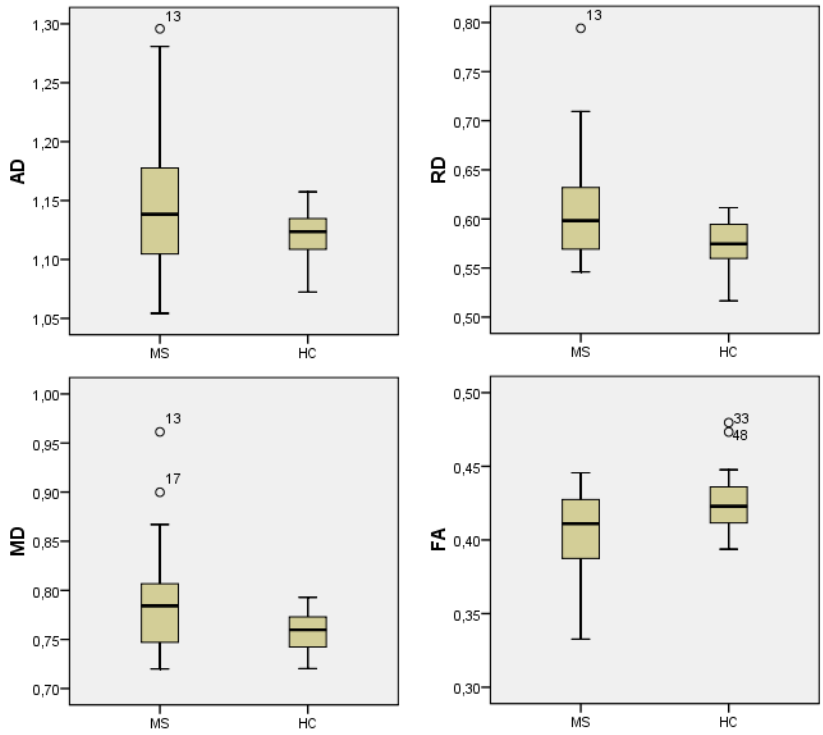

Figure 3.6 Boxplots of AD, RD, MD and FA of SLFT for relapsing-remitting multiple sclerosis and healthy controls

3.1.2.1.6 Uncinate fasciculus

Table 3.6 shows group differences between AD, RD, MD and FA for SLFT. RRMS presented with significantly higher AD, RD, MD and lower FA.

Figure 3.6 shows boxplots of AD, RD, MD and FA for the two groups.

Table 3.7 Uncinate fasciculus measures in healthy controls and relapsing-remitting multiple sclerosis

	RRMS (*N = 32*)	**HC (*N = 30*)**	***p***
	UNC measures		
AD	1.17 (0.03)	1.15 (0.03)	**0.044**
RD	0.65 (0.04)	0.62 (0.02)	**0.008**
MD	0.82 (0.03)	0.80 (0.02)	**0.007**
FA	0.37 (0.03)	0.39 (0.02)	**0.023**

HC: healthy controls; RRMS: relapsing-remitting multiple sclerosis; N: number; UNC: uncinate fasciculus
Data are presented as mean (standard deviation). AD, RD and MD are given in $mm^2/s * 10^{-3}$. FA is a dimensionless index.
p-values were calculated using ANCOVA, controlling for age and sex. Significant differences are shown in bold

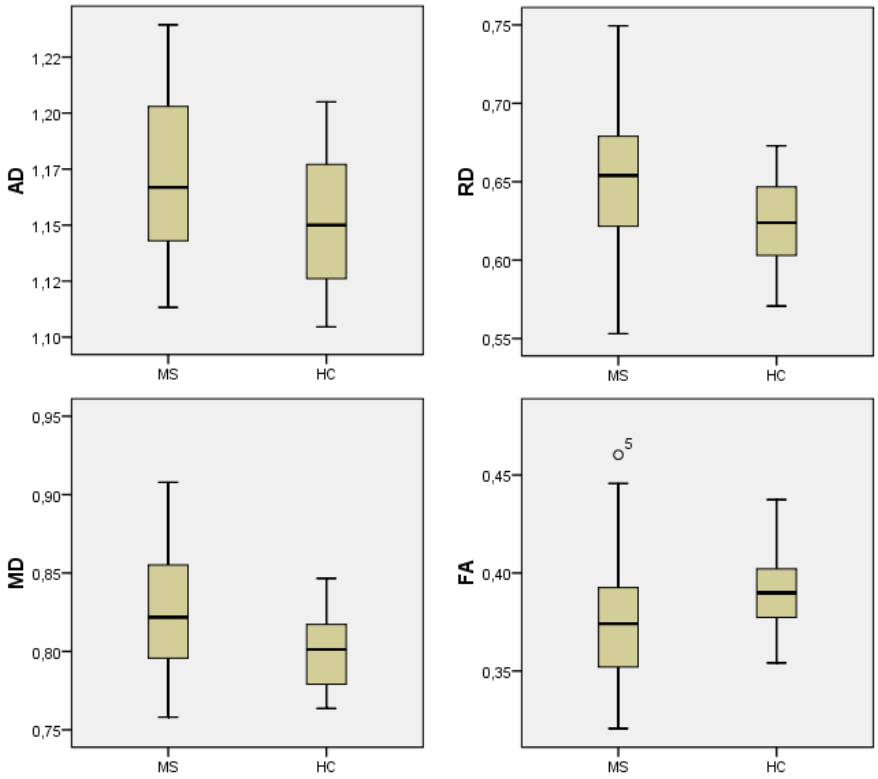

Figure 3.7 Boxplots of AD, RD, MD and FA of UNC for relapsing-remitting multiple sclerosis and healthy controls

3.1.2.2 Cortical measures

ANCOVA models were used to assess groupwise differences in terms of thickness and surface area measures of eleven regions of the cortex.

Caudal and rostral middle frontal gyri, latero-orbital gyrus, superior frontal gyrus, precentral gyrus, supramarginal and superior parietal gyri, lateral occipital gyrus, middle and inferior temporal gyrus and, finally, superior temporal gyrus were chosen, after an attentive analysis of previous works (Catani et al., 2012, Wakana et al., 2004, Catani et al., 2001, Burgel et al. 2005, Thiebaut de Schotten et al., 2010, Lawes et al., 2007, Felten et al., 2004, FitzGerald et al., 2002) matched with an "in-house" method (see section 2.4), as the regions of the cortex to be correlated with the reconstructed tracts.

Table 3.8 and 3.9 shows thickness and surface area measures, respectively, for all the regions of the cortex, and eventually their average, used in this study: although no significant group differences were found, thickness and surface area measures of RRMS group were consistently lower the HC group, as expected from previous studies (Nygaard et al., 2014, Klaver et al., 2013, Zivadinov et al., 2013).

Table 3.8 Cortical thickness measures in healthy controls and relapsing-remitting multiple sclerosis. Interestingly, no statistical significance was found but only a trend of atrophy in MS vs. HC. This finding renders even more important the study on area atrophy to tract damage dealt with in the following paragraph.

	RRMS (*N = 32*)	**HC (*N = 30*)**	***p***
	Thickness measures		
Rostral-middle frontal	2.41 (0.21)	2.49 (0.13)	0.159
Caudal-middle frontal	2.46 (0.22)	2.53 (0.13)	0.283
Middle frontal (avg)	2.42 (0.20)	2.50 (0.13)	0.180
Lateral-orbito frontal	2.73 (0.17)	2.78 (0.12)	0.283
Superior frontal	2.64 (0.25)	2.74 (0.15)	0.499
Inferior temporal	2.89 (0.19)	2.94 (0.13)	0.499
Middle temporal	2.81 (0.18)	2.87 (0.11)	0.165
Inferior-middle temporal (avg)	2.85 (0.18)	2.90 (0.11)	0.277
Superior temporal	2.82 (0.19)	2.91 (0.12)	0.067
Lateral occipital	2.07 (0.12)	2.14 (0.14)	0.072
Supramarginal	2.45 (0.19)	2.52 (0.15)	0.324
Superior parietal	2.09 (0.16)	2.13 (0.12)	0.431
Parietal (avg)	2.24 (0.17)	2.29 (0.11)	0.413
Precentral	2.29 (0.20)	2.39 (0.19)	0.116

HC: healthy controls; RRMS: relapsing-remitting multiple sclerosis; N: number.
Middle frontal (avg): average of rostral-middle frontal and caudal-middle frontal measures;
Inferior-middle temporal (avg): average of inferior temporal and middle temporal measures;
Parietal (avg): average of supramarginal and superior parietal measures.
Data are presented as mean (standard deviation). Thickness measures are given in mm.
p-values were calculated using ANCOVA, controlling for age and sex. Significant differences are shown in bold

Table 3.9 Cortical surface area measures in healthy controls and relapsing-remitting multiple sclerosis

	RRMS (*N = 32*)	**HC (*N = 30*)**	***p***
	Surface area measures		
Rostral-middle frontal	11187 (1880)	11418 (1611)	0.159
Caudal-middle frontal	4265 (772)	4298 (788)	0.241
Middle frontal (avg)	7776 (1270)	7858 (1117)	0.647
Lateral orbitofrontal	5034 (644)	5166 (688)	0.694
Superior frontal	13613 (1993)	14202 (1963)	0.342
Inferior temporal	6252 (767)	6453 (909)	0.767
Middle temporal	6141 (970)	6445 (779)	0.181
Inferior-middle temporal (avg)	6196 (921)	6440 (792)	0.347
Superior temporal	7106 (879)	7321 (886)	0.473
Lateral occipital	9001 (1346)	9697 (1340)	**0.017**
Supramarginal	7427 (1266)	7508 (1107)	0.681
Superior parietal	10184 (1449)	10703 (1256)	0.120
Parietal (avg)	8806 (1296)	9105 (1126)	0.440
Precentral	9756 (1232)	10034 (1084)	0.456

HC: healthy controls; RRMS: relapsing-remitting multiple sclerosis; N: number.
Middle frontal (avg): average of rostral-middle frontal and caudal-middle frontal measures;
Inferior-middle temporal (avg): average of inferior temporal and middle temporal measures;
Parietal (avg): average of supramarginal and superior parietal measures.
Data are presented as mean (standard deviation). Surface area measures are given in mm^2.
p-values were calculated using ANCOVA, controlling for age, sex and total intracranial volume. Significant differences are shown in bold

3.2 **Partial Correlations**

DTI coefficients of white matter tracts were correlated with thickness and surface area measures of the cortex, in order to assess whether damage in white matter in RRMS patients might be associated with atrophy in connected cortical regions with respect to non-connected regions.

3.2.1 *Anterior thalamic radiations*

DTI measures of ATR were correlated with rostral-middle frontal, caudal-middle frontal gyri and with the average of their cortical measures. The lateral occipital gyrus was used for comparison as non-connected region.

Table 3.10 shows correlations with cortical thickness. First, it must be highlighted that significant correlations were found only for RRMS patients, while no significant associations were found for healthy controls, for neither connected regions nor non-connected regions. The same pattern of correlations was found also in all the other tracts analyzed in this study (see next sections).

Moreover, when looking at the RRMS group, three DTI measures (AD, RD and MD) of ATR significantly correlated with cortical thickness of the considered connected regions, while only MD significantly correlated with the thickness of the lateral occipital gyrus, the non-connected region of comparison. Also this trend, characterized by a higher number of correlations with connected regions rather than non-connected ones, was respected by the other five tracts analyzed.

Table 3.11, instead, shows correlations with surface area measures. In this case, the pattern of correlations was not as well defined as it is for thickness, and the same could be said for the other tracts analyzed. In fact, in the various tracts, correlations between DTI coefficients and surface area measures was found for both RRMS patients and healthy controls.

Table 3.10 Partial correlations between DTI measures of ATR and thickness measures of connected and non-connected regions in healthy controls and relapsing-remitting multiple sclerosis

	RRMS (*N = 32*)	**HC (*N = 30*)**
	Rostral-middle frontal thickness	
FA	0,314 (0.091)	0.270 (0.164)
AD	**-0.410 (0.024)**	0.272 (0.162)
RD	**-0,483 (0.007)**	-0.161 (0.413)
MD	**-0,513 (0.004)**	-0.035 (0.858)
	Caudal-middle frontal thickness	
FA	0,171 (0.366)	0.283 (0.144)
AD	**-0.541 (0.002)**	0.224 (0.251)
RD	**-0,429 (0.018)**	-0.205 (0.296)
MD	**-0,522 (0.003)**	-0.090 (0.647)
	Middle frontal (avg) thickness	
FA	0,278 (0.137)	0.290 (0.134)
AD	**-0.465 (0.010)**	0.276 (0.156)
RD	**-0,481 (0.007)**	-0.182 (0.353)
MD	**-0,531 (0.003)**	-0.052 (0.792)
	Lateral occipital thickness (comparison)	
FA	0,226 (0.229)	0.144 (0.465)
AD	-0.303 (0.104)	0.307 (0.113)
RD	-0,350 (0.058)	-0.037 (0.854)
MD	**-0,374 (0.042)**	0.084 (0.671)

HC: healthy controls; RRMS: relapsing-remitting multiple sclerosis; N: number; FA: fractional anisotropy; MD: mean diffusivity; AD: axial diffusivity; RD: radial diffusivity.
Partial correlations were calculated controlling for age and sex.
Data are shown as r (*p*-value), whereas r is the correlation coefficient. Significant correlations are shown in bold

Table 3.11 Partial correlations between DTI measures of ATR and surface area measures of connected and non-connected regions in healthy controls and relapsing-remitting multiple sclerosis

	RRMS (*N = 32*)	**HC (*N = 30*)**
	Rostral-middle frontal surface area	
FA	-0.099 (0.610)	0.008 (0.967)
AD	0.165 (0.391)	**-0.470 (0.013)**
RD	0.153 (0.428)	-0.193 (0.334)
MD	0.176 (0.360)	-0.336 (0.087)
	Caudal-middle frontal surface area	
FA	-0.351 (0.062)	0.319 (0.105)
AD	-0.078 (0.687)	-0.286 (0.149)
RD	0.251 (0.189)	**-0.422 (0.028)**
MD	0.157 (0.415)	**-0.464 (0.015)**
	Middle frontal (avg) surface area	
FA	-0.192 (0.318)	0.149 (0.459)
AD	0.107 (0.581)	**-0.500 (0.008)**
RD	0.203 (0.291)	-0.341 (0.082)
MD	0.192 (0.320)	**-0.473 (0.013)**
	Lateral occipital surface area (comparison)	
FA	-0.046 (0.811)	-0.021 (0.918)
AD	-0.013 (0.946)	**-0.405 (0.036)**
RD	-0.078 (0.686)	-0.149 (0.459)
MD	-0.063 (0.745)	-0.274 (0.166)

HC: healthy controls; RRMS: relapsing-remitting multiple sclerosis; N: number; FA: fractional anisotropy; MD: mean diffusivity; AD: axial diffusivity; RD: radial diffusivity.
Partial correlations were calculated controlling for age, sex and total intracranial volume.
Data are shown as r (*p*-value), whereas r is the correlation coefficient. Significant correlations are shown in bold

3.2.2 *Corticospinal tract*

DTI measures of CST were correlated with cortical measures of precentral gyrus. The lateral occipital gyrus was the non-connected region used as comparison.

Table 3.12 shows correlations with cortical thickness. As underlined in the previous section (3.2.1), no associations were found in healthy controls, while a correlation was found between AD of CST and thickness of precentral gyrus in RRMS patients. No correlations were found with the lateral occipital gyrus.

Table 3.13 shows partial correlations with surface area.

Table 3.12 Partial correlations between DTI measures of CST and thickness measures of connected and non-connected regions in healthy controls and relapsing-remitting multiple sclerosis

	RRMS (*N = 32*)	**HC (*N = 30*)**
	Precentral thickness	
FA	-0,242 (0.198)	0.092 (0.643)
AD	**-0.367 (0.046)**	0.045 (0.818)
RD	0.002 (0.992)	-0.076 (0.702)
MD	-0,168 (0.374)	-0.040 (0.840)
	Lateral occipital thickness (comparison)	
FA	-0,029 (0.880)	-0.090 (0.648)
AD	-0.258 (0.169)	0.145 (0.460)
RD	-0.093 (0.623)	0.173 (0.379)
MD	-0,185 (0.327)	0.211 (0.282)

HC: healthy controls; RRMS: relapsing-remitting multiple sclerosis; N: number; FA: fractional anisotropy; MD: mean diffusivity; AD: axial diffusivity; RD: radial diffusivity.
Partial correlations were calculated controlling for age and sex.
Data are shown as r (*p*-value), whereas r is the correlation coefficient. Significant correlations are shown in bold

Table 3.13 Partial correlations between DTI measures of CST and surface area measures of connected and non-connected regions in healthy controls and relapsing-remitting multiple sclerosis

	RRMS (*N = 32*)	**HC (*N = 30*)**
	Precentral surface area	
FA	-0.152 (0.432)	0.341 (0.081)
AD	0.014 (0.942)	-0.206 (0.304)
RD	0.151 (0.436)	**-0.420 (0.029)**
MD	0.113 (0.561)	**-0.432 (0.024)**
	Lateral occipital surface area (comparison)	
FA	0.009 (0.962)	0.146 (0.467)
AD	-0.145 (0.452)	0.079 (0.695)
RD	-0.104 (0.592)	-0.121 (0.548)
MD	-0.142 (0.464)	-0.060 (0.766)

HC: healthy controls; RRMS: relapsing-remitting multiple sclerosis; N: number; FA: fractional anisotropy; MD: mean diffusivity; AD: axial diffusivity; RD: radial diffusivity.
Partial correlations were calculated controlling for age, sex and total intracranial volume.
Data are shown as r (*p*-value), whereas r is the correlation coefficient. Significant correlations are shown in bold

3.2.3 *Inferior longitudinal fasciculus*

ATR and CST, presented so far, are two projective tracts, thus they connect the cortex with subcortical regions, thalamus and brainstem respectively. Unlike these, ILF, as well as SLFP, SLFT and UNC, are associative tracts, which means they connect two cortical regions of the same hemisphere. This is the reason why these tracts were correlated with connected regions from two different lobes of the brain, besides a non-connected region as comparison.

Therefore, DTI indexes of ILF were correlated, by one side, with inferior temporal and middle temporal gyri and with the average of their cortical measures, and, by the other side, with the lateral occipital gyrus. Fort this tract, the precentral gyrus was used for comparison.

Table 3.14 shows correlations with cortical thickness. FA, RD and MD correlated with the thickness of the inferior temporal and middle temporal gyri and with their average in RRMS patients. AD correlated with middle temporal thickness in healthy controls, and this represented the only correlation found in the whole work between a DTI coefficient and the thickness measure of a healthy control. MD correlated with the thickness of the lateral occipital gyrus in RRMS patients. RD and MD correlated with the thickness of the non-connected region, the precentral gyrus.

Table 3.15 shows correlations with surface area measures.

Table 3.14 Partial correlations between DTI measures of ILF and thickness measures of connected and non-connected regions in healthy controls and relapsing-remitting multiple sclerosis

	RRMS (*N = 32*)	**HC (*N = 30*)**
	Inferior temporal thickness	
FA	**0,373 (0.042)**	0.000 (1.000)
AD	-0.328 (0.077)	0.148 (0.452)
RD	**-0,445 (0.014)**	0.061 (0.756)
MD	**-0,448 (0.013)**	0.131 (0.508)
	Middle temporal thickness	
FA	**0,436 (0.016)**	0.349 (0.068)
AD	-0.305 (0.101)	**0.470 (0.012)**
RD	**-0,476 (0.008)**	-0.117 (0.552)
MD	**-0,463 (0.010)**	-0.180 (0.359)
	Inferior-middle temporal (avg) thickness	
FA	**0,421 (0.021)**	0.177 (0.369)
AD	-0.329 (0.076)	0.336 (0.081)
RD	**-0,480 (0.007)**	-0.017 (0.930)
MD	**-0,474 (0.008)**	0.179 (0.363)
	Lateral occipital thickness	
FA	0,297 (0.110)	0.217 (0.268)
AD	-0.315 (0.089)	0.309 (0.109)
RD	-0,349 (0.058)	-0. 083(0.675)
MD	**-0,372 (0.043)**	0.114 (0.563)
	Precentral thickness (comparison)	
FA	0,324 (0.080)	0.139 (0.480)
AD	-0.362 (0.050)	0.275 (0.156)
RD	**-0,432 (0.017)**	-0.032 (0.873)
MD	**-0,450 (0.013)**	-0.032 (0.873)

HC: healthy controls; RRMS: relapsing-remitting multiple sclerosis; N: number; FA: fractional anisotropy; MD: mean diffusivity; AD: axial diffusivity; RD: radial diffusivity.
Partial correlations were calculated controlling for age and sex.
Data are shown as r (*p*-value), whereas r is the correlation coefficient. Significant correlations are shown in bold

Table 3.15 Partial correlations between DTI measures of ILF and surface area measures of connected and non-connected regions in healthy controls and relapsing-remitting multiple sclerosis

	RRMS (*N = 32*)	**HC (*N = 30*)**
	Inferior temporal surface area	
FA	-0.275 (0.149)	-0.048 (0.811)
AD	0.162 (0.401)	-0.270 (0.173)
RD	0.302 (0.111)	-0.043 (0.832)
MD	0.281 (0.139)	-0.177 (0.378)
	Middle temporal surface area	
FA	-0.078 (0.687)	0.107 (0.596)
AD	0.128 (0.508)	-0.111 (0.583)
RD	0.134 (0.487)	-0.121 (0.547)
MD	0.145 (0.452)	-0.157 (0.433)
	Inferior-middle temporal (avg) surface area	
FA	0.028 (0.889)	-0.192 (0.318)
AD	-0.251 (0.206)	0.159 (0.410)
RD	-0.100 (0.621)	0.239 (0.213)
MD	-0.214 (0.284)	0.233 (0.223)
	Lateral occipital surface area	
FA	0.158 (0.431)	0.111 (0.568)
AD	0.070 (0.729)	-0.083 (0.667)
RD	-0.144 (0.473)	0.172 (0.371)
MD	-0.082 (0.685)	-0.157 (0.416)
	Precentral surface area (comparison)	
FA	0.322 (0.101)	-0.250 (0.190)
AD	-0.250 (0.208)	-0.046 (0.811)
RD	**-0.457 (0.017)**	0.165 (0.392)
MD	**-0.506 (0.007)**	0.105 (0.588)

HC: healthy controls; RRMS: relapsing-remitting multiple sclerosis; N: number; FA: fractional anisotropy; MD: mean diffusivity; AD: axial diffusivity; RD: radial diffusivity.
Partial correlations were calculated controlling for age, sex and total intracranial volume.
Data are shown as r (*p*-value), whereas r is the correlation coefficient. Significant correlations are shown in bold

3.2.4 *Superior longitudinal fasciculus – parietal endings*

DTI measures of SLFP were correlated, by one side, with cortical measures of superior parietal and supramarginal gyri and with their average, as well as, by the other side, with superior frontal gyrus. The lateral occipital gyrus was used for comparison.

Table 3.16 shows correlations with cortical thickness. FA correlated with the thickness of supramarginal, superior parietal and superior frontal gyri, and with the parietal average as well. RD correlated with supramarginal gyrus, with the parietal average and with the superior frontal gyrus but did not with superior parietal gyrus. MD correlated only with supramarginal gyrus. No associations were found with lateral occipital thickness.

Table 3.17 shows correlations with surface area measures.

Table 3.16 Partial correlations between DTI measures of SLFP and thickness measures of connected and non-connected regions in healthy controls and relapsing-remitting multiple sclerosis

	RRMS (*N = 32*)	**HC (*N = 30*)**
	Supramarginal thickness	
FA	**0,442 (0.015)**	0.080 (0.686)
AD	-0.268 (0.152)	0.231 (0.237)
RD	**-0,398 (0.029)**	0.017 (0.931)
MD	**-0,365 (0.047)**	-0.087 (0.659)
	Superior parietal thickness	
FA	**0,434 (0.016)**	0.069 (0.726)
AD	-0.185 (0.327)	-0.058 (0.769)
RD	-0,316 (0.089)	-0.081 (0.680)
MD	-0,280 (0.134)	-0.084 (0.673)
	Parietal (avg) thickness	
FA	**0,468 (0.009)**	0.078 (0.694)
AD	-0.225 (0.233)	0.079 (0.691)
RD	**-0,372 (0.043)**	-0.034 (0.864)
MD	-0,331 (0.074)	-0.002 (0.992)
	Superior frontal thickness	
FA	**0,297 (0.042)**	0.063 (0.751)
AD	-0.268 (0.151)	0.227 (0.245)
RD	**-0,376 (0.040)**	0.022 (0.910)
MD	-0,351 (0.058)	0.090 (0.649)
	Lateral occipital thickness (comparison)	
FA	0,355 (0.055)	0.176 (0.371)
AD	-0.168 (0.376)	0.095 (0.630)
RD	-0,258 (0.168)	-0.109 (0.581)
MD	-0,234 (0.212)	-0.057 (0.774)

HC: healthy controls; RRMS: relapsing-remitting multiple sclerosis; N: number; FA: fractional anisotropy; MD: mean diffusivity; AD: axial diffusivity; RD: radial diffusivity.
Partial correlations were calculated controlling for age and sex.
Data are shown as r (*p*-value), whereas r is the correlation coefficient. Significant correlations are shown in bold

Table 3.17 Partial correlations between DTI measures of SLFP and surface area measures of connected and non-connected regions in healthy controls and relapsing-remitting multiple sclerosis

	RRMS (*N = 32*)	**HC (*N = 30*)**
	Supramarginal surface area	
FA	-0.213 (0.268)	0.257 (0.196)
AD	0.053 (0.786)	-0.039 (0.848)
RD	0.113 (0.560)	-0.205 (0.305)
MD	0.095 (0.624)	-0.177 (0.378)
	Superior parietal surface area	
FA	**-0.444 (0.016)**	0.274 (0.166)
AD	0.054 (0.781)	0.136 (0.500)
RD	0.254 (0.184)	-0.218 (0.276)
MD	0.190 (0.322)	-0.132 (0.510)
	Parietal (avg) surface area	
FA	**-0.389 (0.037)**	0.310 (0.115)
AD	0.060 (0.755)	0.061 (0.761)
RD	0.218 (0.256)	-0.247 (0.215)
MD	0.168 (0.382)	-0.179 (0.372)
	Superior frontal surface area	
FA	-0.163 (0.397)	0.441 (0.021)
AD	-0.095 (0.626)	0.031 (0.877)
RD	0.001 (0.998)	-0.365 (0.061)
MD	-0.034 (0.861)	-0.284 (0.152)
	Lateral occipital surface area (comparison)	
FA	0.048 (0.806)	0.067 (0.742)
AD	-0.356 (0.058)	-0.029 (0.886)
RD	-0.249 (0.192)	-0.098 (0.627)
MD	-0.297 (0.118)	-0.088 (0.664)

HC: healthy controls; RRMS: relapsing-remitting multiple sclerosis; N: number; FA: fractional anisotropy; MD: mean diffusivity; AD: axial diffusivity; RD: radial diffusivity.
Partial correlations were calculated controlling for age and sex.
Data are shown as r (*p*-value), whereas r is the correlation coefficient. Significant correlations are shown in bold

3.2.5 *Superior longitudinal fasciculus – temporal endings*

DTI measures of SLFT were correlated, by one side, with cortical measures of superior temporal gyrus and, by the other side, with superior frontal gyrus. The lateral occipital gyrus was used for comparison.

Table 3.18 shows correlations with cortical thickness. FA and RD correlated with the thickness of superior temporal and superior frontal gyri, and with the parietal average as well. MD correlated with superior frontal gyrus. FA was also associated with lateral occipital thickness.

Table 3.19 shows partial correlations with surface area measures.

Table 3.18 Partial correlations between DTI measures of SLFT and thickness measures of connected and non-connected regions in healthy controls and relapsing-remitting multiple sclerosis

	RRMS (*N = 32*)	**HC (*N = 30*)**
	Superior temporal thickness	
FA	**0,474 (0.008)**	0.106 (0.592)
AD	-0.228 (0.225)	0.336 (0.081)
RD	**-0,386 (0.035)**	0.032 (0.872)
MD	-0,344 (0.062)	0.138 (0.484)
	Superior frontal thickness	
FA	**0,415 (0.023)**	-0.034 (0.864)
AD	-0.275 (0.141)	0.148 (0.453)
RD	**-0,415 (0.023)**	0.061 (0.759)
MD	**-0,380 (0.038)**	0.098 (0.619)
	Lateral occipital thickness (comparison)	
FA	**0,378 (0.039)**	0.282 (0.147)
AD	-0.256 (0.172)	0.234 (0.231)
RD	-0,338 (0.068)	-0.167 (0.397)
MD	-0,320 (0.085)	-0.056 (0.778)

HC: healthy controls; RRMS: relapsing-remitting multiple sclerosis; N: number; FA: fractional anisotropy; MD: mean diffusivity; AD: axial diffusivity; RD: radial diffusivity.
Partial correlations were calculated controlling for age, sex and total intracranial volume.
Data are shown as r (*p*-value), whereas r is the correlation coefficient. Significant correlations are shown in bold

Table 3.19 Partial correlations between DTI measures of SLFT and surface area measures of connected and non-connected regions in healthy controls and relapsing-remitting multiple sclerosis

	RRMS (*N = 32*)	**HC (*N = 30*)**
	Superior temporal surface area	
FA	-0.192 (0.319)	0.216 (0.280)
AD	0.026 (0.894)	-0.055 (0.784)
RD	0.081 (0.678)	-0.195 (0.329)
MD	0.065 (0.739)	-0.179 (0.371)
	Superior frontal surface area	
FA	-0.133 (0.493)	0.402 (0.038)
AD	-0.026 (0.894)	0.024 (0.906)
RD	0.047 (0.807)	-0.356 (0.069)
MD	0.024 (0.901)	-0.289 (0.144)
	Lateral occipital surface area (comparison)	
FA	0.030 (0.878)	0.097 (0.630)
AD	**-0.374 (0.045)**	-0.122 (0.545)
RD	-0.234 (0.222)	-0.156 (0.437)
MD	-0.289 (0.129)	-0.167 (0.406)

HC: healthy controls; RRMS: relapsing-remitting multiple sclerosis; N: number; FA: fractional anisotropy; MD: mean diffusivity; AD: axial diffusivity; RD: radial diffusivity.
Partial correlations were calculated controlling for age, sex and total intracranial volume.
Data are shown as r (*p*-value), whereas r is the correlation coefficient. Significant correlations are shown in bold

3.2.6 *Uncinate fasciculus*

DTI measures of UNC were correlated, by one side, with inferior temporal, middle temporal gyri and with the average of their cortical measures, while, by the other side, with lateral orbitofrontal gyrus. The superior parietal gyrus was used for comparison.

Table 3.20 shows correlation with cortical thickness. Also this time the "usual" pattern of correlations presented in 3.2.1 was respected: AD, RD and MD correlated with the cortical thickness of all the connected regions. No associations were found with the thickness of the non-connected region, the superior parietal gyrus.

Table 3.21 shows partial correlations with surface area measures.

Table 3.20 Partial correlations between DTI measures of UNC and thickness measures of connected and non-connected regions in healthy controls and relapsing-remitting multiple sclerosis

	RRMS (*N = 32*)	**HC (*N = 30*)**
	Inferior temporal thickness	
FA	0,284 (0.128)	-0.069 (0.728)
AD	**-0.467 (0.009)**	-0.122 (0.536)
RD	**-0,435 (0.016)**	0.016 (0.934)
MD	**-0,479 (0.007)**	-0.039 (0.846)
	Middle temporal thickness	
FA	0,221 (0.241)	0.194 (0.322)
AD	**-0.429 (0.018)**	0.164 (0.403)
RD	**-0,372 (0.043)**	-0.106 (0.591)
MD	**-0,419 (0.021)**	-0.009 (0.962)
	Inferior-middle temporal (avg) thickness	
FA	0,260 (0.165)	0.054 (0.785)
AD	**-0.468 (0.009)**	0.013 (0.948)
RD	**-0,419 (0.021)**	-0.040 (0.839)
MD	**-0,467 (0.009)**	-0.024 (0.903)
	Lateral orbitofrontal thickness	
FA	0,294 (0.115)	0.080 (0.687)
AD	**-0.397 (0.030)**	0.137 (0.487)
RD	**-0,431 (0.017)**	0.000 (1.000)
MD	**-0,453 (0.012)**	0.057 (0.775)
	Superior parietal thickness (comparison)	
FA	0,301 (0.106)	0.197 (0.314)
AD	-0.284 (0.128)	0.128 (0.515)
RD	-0,355 (0.054)	-0.134 (0.497)
MD	-0,359 (0.052)	-0.045 (0.821)

HC: healthy controls; RRMS: relapsing-remitting multiple sclerosis; N: number; FA: fractional anisotropy; MD: mean diffusivity; AD: axial diffusivity; RD: radial diffusivity.
Partial correlations were calculated controlling for age and sex.
Data are shown as r (*p*-value), whereas r is the correlation coefficient. Significant correlations are shown in bold

Table 3.21 Partial correlations between DTI measures of UNC and surface area measures of connected and non-connected regions in healthy controls and relapsing-remitting multiple sclerosis

	RRMS (*N = 32*)	**HC (*N = 30*)**
	Inferior temporal surface area	
FA	**-0.497 (0.006)**	-0.001 (0.995)
AD	0.190 (0.324)	-0.211 (0.290)
RD	**0.456 (0.013)**	-0.093 (0.644)
MD	**0.396 (0.033)**	-0.152 (0.450)
	Middle temporal surface area	
FA	-0.310 (0.102)	0.163 (0.418)
AD	0.104 (0.591)	0.142 (0.481)
RD	0.297 (0.118)	-0.047 (0.815)
MD	0.251 (0.188)	0.023 (0.910)
	Inferior-middle temporal (avg) surface area	
FA	**-0.442 (0.016)**	0.093 (0.645)
AD	0.161 (0.405)	-0.065 (0.747)
RD	**0.412 (0.026)**	-0.092 (0.649)
MD	0.354 (0.059)	-0.092 (0.647)
	Lateral orbitofrontal surface area	
FA	-0.188 (0.330)	0.390 (0.045)
AD	-0.036 (0.853)	-0.065 (0.746)
RD	0.121 (0.531)	-0.316 (0.108)
MD	0.076 (0.696)	-0.254 (0.202)
	Superior parietal surface area (comparison)	
FA	-0.316 (0.095)	0.028 (0.888)
AD	0.228 (0.234)	-0.171 (0.394)
RD	0.334 (0.077)	-0.169 (0.400)
MD	0.321 (0.090)	-0.190 (0.343)

HC: healthy controls; RRMS: relapsing-remitting multiple sclerosis; N: number; FA: fractional anisotropy; MD: mean diffusivity; AD: axial diffusivity; RD: radial diffusivity.
Partial correlations were calculated controlling for age and sex.
Data are shown as r (*p*-value), whereas r is the correlation coefficient. Significant correlations are shown in bold

3.3 **Multiple Linear Regression**

In the RRMS group, multiple linear regression (MLR) analysis was used to analyze whether the diffusivity metrics of a connected tracts were more predictive of cortical thickness than the contribution of those in a not-connected tract

Thus, for each lobe of the brain, the thickness of a gyrus was chosen as the dependent variable; then multiple linear regressions were divided in two steps: in the first one, only age and sex were included, while, in the second one, DTI metrics of a connected and of a non-connected tract were chosen as possible predictors.

3.3.1 *Occipital lobe*

DTI indexes of the ILF, as connected tract, and those of the UNC, as non-connected comparison tract, were used to predict the cortical thickness of the lateral occipital gyrus.

The first step of the model retained only age as a significant predictors, but the model was not a significant fit of the overall data (p = 0.098). With the inclusion of MD of the ILF as predictor, the model became significant, with an increase of the amount of the variance in the outcome explained by the model of about 10% (adjusted R^2 from 0.089 to 0.188). In addition, F increased, meaning a rise in the ratio between the explained part of the data, from fitting the model, relative to the unexplained amount.

No other DTI indexes of neither ILF nor UNC were retained in the model, meaning that the inclusion of another index would not have changed the amount of variance explained by the model.

Table 3.22 Significant variables in predicting the cortical thickness of the lateral occipital gyrus. In the first step only covariates, age and sex, were included, while, in the second step, DTI indexes of ILF (connected tract) and UNC (non-connected tract) were evaluated as possible predictors.

	β	***p***
Step 1		
AGE	-0.423	**0.033**
Step 2		
AGE	-0.441	**0.019**
ILF MD	-0.347	**0.043**

β: regression coefficient; ILF MD: mean diffusivity of the ILF.
Only significant predictors are shown.
Step 1: adj. R^2=0.089; F=2.523; *p*=0.098;
Step 2: adj. R^2=0.188; F=3.387; *p*=**0.032**.

3.3.2 *Temporal lobe*

DTI indexes of the ILF and of the UNC, as connected tracts, and those of the SLFP, as non-connected comparison tract, were used to predict the average thickness of the middle and the inferior temporal gyri.

In the first step of the model only age was retained as significant predictor, while, in the second step RD of ILF was added. Adjusted R^2 increased from 0.154 to 0.325, bringing to an increase of the amount of variance in the outcome explained by the model of about 17%. F-ratio increased, as well.

No other DTI indexes of neither ILF, UNC nor SLFP were retained in the model.

Table 3.23 Significant variables in predicting the average thickness of the middle and of the inferior temporal gyri. In the first step only covariates, age and sex, were included, while, in the second step, DTI indexes of ILF, UNC (connected tracts) and SLFP (non-connected tract) were evaluated as possible predictors.

	β	***p***
Step 1		
AGE	-0.392	**0.039**
Step 2		
AGE	-0.415	**0.016**
ILF RD	-0.428	**0.007**

β: regression coefficient; ILF RD: radial diffusivity of the ILF.
Only significant predictors are shown.
Step 1: adj. R^2=0.154; F=3.824; *p*=**0.034**;
Step 2: adj. R^2=0.325; F=5.985; *p*=**0.003**.

3.3.3 *Frontal lobe*

DTI indexes of the SLFP and of the SLFT, as connected tracts, and those of the CST, as a non-connected comparison tract, were used to predict the thickness of the superior frontal gyrus.

In the first step of the model only age was retained as significant predictor, while, in the second step RD of SLFT was added. Adjusted R^2 increased from 0.21 to 0.307, bringing to an increase of the amount of variance in the outcome explained by the model of about 10%. F-ratio increased, as well.

No other DTI indexes of neither SLFT, SLFP nor CST were retained in the model.

Table 3.24 Significant variables in predicting the cortical thickness of the superior frontal gyrus. In the first step only covariates, age and sex, were included, while, in the second step, DTI indexes of SLFT, SLFP (connected tracts) and CST (non-connected tract) were evaluated as possible predictors.

	β	***p***
Step 1		
AGE	-0.437	**0.002**
Step 2		
AGE	-0.324	**0.007**
SLFT RD	-0.348	**0.004**

β: regression coefficient; SLFT RD: radial diffusivity of the SLFT.
Only significant predictors are shown.
Step 1: adj. R^2=0.210; F=9.126; p<**0.001**;
Step 2: adj. R^2=0.307; F=10.012; p<**0.001**.

3.3.4 *Parietal lobe*

DTI indexes of the SLFP, as connected tract, and those of the UNC, as a non-connected comparison tract, were used to predict the average of the thickness of the supramarginal and of the superior parietal gyri.

In the first step of the model only age was retained as significant predictor, while, in the second step FA of SLFP was added as well. Adjusted R^2 increased from 0.167 to 0.253, bringing to an increase of the amount of variance in the outcome explained by the model of about 10%. F-ratio increased, as well.

No other DTI indexes of neither SLFP nor UNC were retained in the model.

Table 3.25 Significant variables in predicting the average thickness of the supramarginal and of the superior parietal gyri. In the first step only covariates, age and sex, were included, while, in the second step, DTI indexes of ILF, UNC (connected tracts) and SLFP (non-connected tract) were evaluated as possible predictors.

	β	***p***
Step 1		
AGE	-0.437	**0.002**
Step 2		
AGE	-0.324	**0.007**
SLFP FA	-0.348	**0.004**

β: regression coefficient; SLFP FA: fractional anisotropy of the SLFP.
Only significant predictors are shown.
Step 1: adj. R^2=0.167; F=7.128; p=**0.002**;
Step 2: adj. R^2=0.253; F=7.897; p<**0.001**.

4. DISCUSSION

4.1 **Healthy controls and patients comparison**

Thirty healthy controls (HC) and thirty-two relapsing-remitting multiple sclerosis (RRMS, or briefly MS) patients were enrolled in this study, which aimed to analyze the relationship between WM injury and atrophy in both connected and non-connected regions of cortical GM.

4.1.1 *DTI measures*

Significant differences were found between groups in the tracts that were tested. As shown in the Table 3.2Table 3.3Table 3.4Table 3.5Table 3.6Table 3.7 the DTI measures of each WM bundle of RRMS patients were characterized by increased AD, MD and RD and decreased FA with respect to HC. In particular AD was significantly increased in each tract with the exception of the ILF, RD was significantly higher in each tract with the exception of the ATR, MD was significantly higher in each tract, while FA showed the expected decreasing trend but no significant differences were found in the SLFP, the CST, and the ATR. To gain deeper insights in these results we have to understand what the aforementioned DTI measures represent. It must be highlighted that there are several opinions with respect to their exact interpretation. Some (Filippi et al., 2001, Sbardella et al., 2013) have proposed that DTI-derived parameters are specific to the underlying type of damage, reports have demonstrated that such interpretations need to be made with much caution (Wheeler-Kingshott and Cercignani, 2009), at least for what regards AD and RD. This is particularly true in the case of voxels with multiple fiber populations. E.g., recent work has demonstrated that potentially up to 90 percent of WM voxels showing a univocal direction in DTI may contain at least two distinct fiber directions due to fiber crossing when analyzed by high angular resolution diffusion imaging techniques (Jeurissen et al., 2013). Similarly, the application of advanced high b-value techniques with multi-

compartment modeling has shown the reach distribution of fiber calibers and types (Assaf et al., 2008).

AD, which reflects the diffusion parallel to the fibers, might be linked to axonal transection in MS (Buddle et al., 2009), but contrasting findings were reported in literature (Fink et al., 2009). Decreased AD might be associated with the typical axonal loss and fragmentation present in MS. However, higher AD in MS patients with respect to HC has also been reported (Liu et al.,2012; Bergsland et al., 2015) . In this scenario, increased AD might be related to compensatory mechanisms used to maintain functionality in presence of WM damage (Sbardella et al., 2013). Thus, the timeline of the disease could play some role since the initial damage might cause a decrease in AD, followed by a compensative assessment leading to its increase, which, nevertheless, could also be linked to the overall increase in mean diffusivity evidenced in MS.

It is more intuitive, but still uncertain (Wheeler-Kingshott and Cercignani, 2009), to link the RD to the high demyelination caused by the MS disease. RD represents the average of the two minor eigenvalue of the diffusion tensor, thus its increase in WM tracts of MS patients might be due to the loss of myelin (Song et al., 2002), which allows for a higher degree of diffusion in the directions perpendicular to the fibers.

MD and FA are the most used DTI metrics as they both derive from an arithmetical combination of the three eigenvalues associated to the eigenvectors of the tensor.

MD measures the overall amount of water motion without any preferential directionality. The causes of this phenomenon might be linked to all the processes that increase the free space for the movement of water, such as vasogenic edema, a type of cerebral edema in which the blood-brain barrier is disrupted (Stadnik et al., 2003), besides axonal and myelin loss (Sbardella et al., 2013). In fact, it is very unlikely that MD was only by chance higher in MS patients with respect to the HC group for all of the six analyzed tracts.

At last, FA reflects with a scalar value ranging between zero and one, the relative prevalence of one direction of diffusivity with respect to the other two. This metric is retained to be highly affected by the myelin content (Kolasinski et al., 2007). In fact significant FA differences have been observed between myelinated and non-myelinated nerves (Werring et al., 1999). Therefore, a decrease in the degree of

myelination would potentially result in lower FA. However, a wide range of other pathological processes, such as edema, inflammation or gliosis could, also cause a drop in the anisotropy, as stated in the review of Sbardella et al. One should also remember that FA would remain relatively unaffected in the event that AD and RD both increase in a similar magnitude. It is noteworthy that only three tracts on six presented with a significantly reduced FA in MS group with respect to HC, thus this might support the notion that FA may be less sensitive than diffusion coefficient indexes to the amount of underlying tissue damage (Bergsland et al., 2015).

4.1.2 *Cortical measures*

ANCOVA models were also used to assess groupwise differences for thickness and surface area measures of eleven cortical regions.

Table 3.8 and Table 3.9 show reduced, though not significantly, measures of thickness and surface area in MS patients with respect to HC in all the examined regions (except for surface area of the lateral occipital gyrus). This is in line with the notion that cortical atrophy is an important feature of MS, which occurs since the earliest phases of the disease (Calabrese et al., 2009). Neither is surprising, looking deeper in the numbers, that group differences in thickness are more evident than group differences in surface area; in fact cortical thinning is more consistently reported (Narayana et al., 2012; Nygaard et al., 2015; Jehne et al., 2015; Pareto et al., 2015) than reductions in surface area in MS.

4.1.3 *Partial correlations*

The core of the presented work consisted in correlating the aforementioned DTI indexes (AD, RD, MD and FA) from six selected WM tracts with the thickness and the surface area measures of connected and non-connected regions of the cortex.

Particularly, this study took inspiration from a recent findings of Bergsland et al. (2015),though limited to the CST. In fact, they found that, when investigating the MS group, the three diffusivity metrics (AD, RD and MD) of the CST correlated with the cortical thickness of the anatomically and functionally connected PMC, , but did not correlate with a non-connected area of the cortex, such as the PAC. On the other hand, no associations were found between cortical thickness and diffusivity parameters in the HC group . Therefore, the current study aimed to assess whether similar

associations could be detected between cortical areas and connected WM fiber bundles throughout the brain.

Table 4.1 summarizes to the benefit of the discussion correlation results detailed in Table 3.10Table 3.12Table 3.14Table 3.16Table 3.18,Table 3.20. It presents the number of DTI measures, among the four evaluated (AD, MD, RD and FA), whose change in each WM tract correlated with the cortical thickness of connected and non-connected GM area. It is recalled that the projective pathways, ATR and CST, were correlated with one cortical region, while the association tracts, ILF, SLFP, SLFT and UNC, were correlated with the two areas at their endings. Finally, comparisons were made with areas known to be not connected.

Table 4.1 Number of significant correlations found out of four DTI measures of the six tracts and the thickness of the "Connected regions" (left). Comparison with a different, non-connected, cortical area is also shown (right)

	Connected regions				**Comparison**	
	HC	RRMS	HC	RRMS	HC	RRMS
	Middle frontal				Lateral occipital	
ATR	0	3			0	1
	Precentral				Lateral occipital	
CST	0	1			0	0
	Middle-inferior temporal		Lateral occipital		Precentral	
ILF	0	3	0	1	0	2
	Parietal		Superior frontal		Occipital	
SLFP	0	2	0	2	0	0
	Superior temporal		Superior frontal		Occipital	
SLFT	0	2	0	3	0	1
	Middle-inferior temporal		Lateral orbitofrontal		Parietal	
UNC	0	3	0	3	0	0

HC: healthy controls; RRMS: relapsing-remitting multiple sclerosis; ATR: anterior thalamic radiations; CST: corticospinal tract; ILF: inferior longitudinal fasciculus; SLFP: superior longitudinal fasciculus-parietal endings; SLFT: superior longitudinal fasciculus-temporal endings; UNC: uncinate fasciculus.

First, it should be highlighted that no correlations were found in GM-WM connections in the HC group, as expected. Conversely, in RRMS a number of correlations were found between WM damage via the four DTI metrics and the cortical thickness of the region(s) upon which the considered tracts are known to impinge. Moreover, the DTI indexes that did not correlate with the thickness of connected regions correspond to the same ones that were not significantly different from HC by the ANCOVA models. Indeed, it cannot be excluded that damage of some considered tract could be poorly expressed in our RRMS group for many reasons: inherently less affected structure, structure with a late damage, or, trivially, the relatively small size of this study.

In addition, to assess whether similar correlations could be found throughout the brain, regardless of the actual anatomical link between WM bundles and GM cortex, we also analyzed the correlation of each tract with a non-connected region. As reported in the last two columns of Table 4.1, the DTI measures of the CST, SLFP and of the UNC did not correlate with the thickness of the comparison region, while some "spurious" associations were observed for the ATR, ILF, and for the SLFT. This evidence is not surprising, given the widespread MS damage, affecting both WM and GM with an extent correlated with the disease progression, thus introducing an a-priori correlation, which confounds the localized analyses. This consideration suggested the multivariate regressions discussed in the next par. Moreover, future work could profitably address multiple regressions (e.g., by the generalized linear modeling, GLM) either considering partial correlations of the connected area, within a regression vs. all areas or inserting one or more MS progression indexes as covariates(s): amnestic, clinical such as lesional load, overall GM damage, overall WM damage.

The same partial correlations were also analyzed with cortical surface area measures. In this case, though, a clear pattern of associations was not observed. In fact, we found correlations in both HC and MS groups for both connected and non-connected regions. However, as already mentioned, cortical thickness, rather than surface area, appears to be a more relevant feature for describing GM atrophy in MS. Nevertheless Bergsland et al. (2015) reported a significant correlation between the AD and the MD of the CST, the only tract they analyzed, with the surface area of the precentral gyrus in HC group, while no relationships were found for the MS patients.

Thus, the interpretation of the associations between DTI-derived parameters within WM tracts and surface area of the connected GM remains somewhat difficult at this time and correlations (if any) seem more related to the individual physiological diversity rather than MS damage.

4.1.4 *Multiple linear regressions*

We used MLR models to investigate the amount of variance in cortical thinning explained by integrity of the connected WM, performed trying to predict in the MS group the cortical thickness of different regions of the cortex starting from AD, MD, RD and FA of both connected and non-connected WM tracts, besides sex and age of the patients.

The model consistently retained age in addition to one (twice MD, once FA and RD) of the DTI measures from one of the connected WM pathways, but no significance was found vs. the control (not-connected) tract. Thus, a larger correlation significance of cortical thickness in a specific region and a DTI measure of an anatomically linked WM tract was obtained. This finding underlines the importance of studying the relationships between WM tracts and anatomically/functionally connected GM to further understand MS pathogenic mechanisms.

All these evidences are in line with the reports from Bergsland et al., (2015) and they highlight the association between WM injury and atrophy in connected cortical regions in MS. This is an active area of research, as the exact causes of neurodegeneration remain relatively poorly understood. Some (Sepulcre et al., 2013) have argued that GM atrophy is heavily a consequence of damage in the WM (i.e. retrograde neurodegeneration) whereas others have demonstrated a role of pathological processes directly within the GM (Calabrese et al, 2015; Lassmann 2012). Due to the cross-sectional nature of our study, we are unable to unravel the temporal dynamics of the relationships between WM and GM injury. Nonetheless, given the relatively modest amount of variance explained in the MLR models, it seems unlikely that WM damage can be the only cause of GM atrophy. .

5. CONCLUSIONS

This work analyzed the role assumed by the local connections between WM fiber bundles and GM regions of the cortex in the widespread diffusion of the injury throughout the brain in MS disease.

To this aim, we made use of FreeSurfer to have a state of the art segmentation of the cortex and automatically parcellate it; this permitted us to derive morphological measures, such as thickness and surface area, of anatomically distinct regions. Then we used TRACULA, a global probabilistic toolbox, to reconstruct the major WM pathways of the brain, combining DW-images with the aforementioned segmentation of the cortex.

We demonstrated that tissue microstructure alterations in six fundamental WM tracts, represented by significant differences of the DTI measure (AD, MD, RD and FA) between MS patients and HC, are associated with thinning of connected cortical regions.

To the best of our knowledge, the present study was one of the first to investigate the correlations between several WM tracts and connected and non-connected cortical regions in addition to having a HC group for comparison purposes. In fact, we began this work to understand whether previous findings regarding individual association of local GM atrophy to connected WM tracts injury could be extended to other areas throughout the brain. Therefore, our findings underline the relevance of investigating anatomically and functionally related areas of the brain to better understand the widespread damage in MS. Furthermore, they highlight the improved specificity of investigation by means of new tools for GM segmentation and probabilistic WM tract localization.

5.1 **Future developments**

In the current study, we used DTI-derived parameters weighted by the probability of belonging to the corresponding tract. This was done for both the HC and the MS group. Thus, also in the case of a MS patient, each voxel was considered the same without defining whether it was part of an area characterized by focal lesions (FL) or it was effectively part of the so-called normal appearing white matter (NAWM). Previous works reported differences between FL and NAWM, surprisingly demonstrating a higher correlation of the latter with the cortical thinning of connected GM regions. Therefore, a future development might be the inclusion in the processing stream of a mask that would allow to separate the effects within FL from those within the NAWM. This would allow for a more precise characterization of how WM damage relates to cortical thinning in MS.

Another important issue that future developments might test is whether the use of a higher number of directions during the DW acquisitions would affect the results. In fact, in the present work, the distribution of the *ball-and-stick* model at each voxel (see 1.3.3) were estimated from DW data characterized by 12 gradient directions, while nowadays diffusion studies are often based on acquisitions with many more (e.g. 30, 64 or even 256 gradient directions). This was not possible for the current work as it was based on images acquired as part of the clinical routine. However, dedicated research protocols in MR Laboratory of the 'Don Carlo Gnocchi Foundation' have already been initiated with a more advanced acquisition scheme.

A further refinement, as previously mentioned, should address a better separation of damage in specific WM-GM circuits vs. global damage and individual disease progression effects inside the observed WM to GM correlations.

Future developments should also investigate the associations between the effect of WM damage and cortical atrophy in relation to relevant cognitive/functional assessments. Such an analysis may shed further light on possible compensatory mechanisms involved in the face of the widespread damaged caused by the disease.

Finally, it should be underlined that the relationships we found between GM atrophy and WM microstructural damage does not provide information on cause-effect links. Thus, longitudinal studies are warranted to better understand the temporal

dynamics between the two damage and, possibly, indicate which of the two aspects anticipates the other.

BIBLIOGRAPHY

AUDOIN, B., RANJEVA, J., DUONG, M. V. A., IBARROLA, D., MALIKOVA, I., CONFORT-GOUNY, S., ET AL. (2004). VOXEL-BASED ANALYSIS OF MTR IMAGES: A METHOD TO LOCATE GRAY MATTER ABNORMALITIES IN PATIENTS AT THE EARLIEST STAGE OF MULTIPLE SCLEROSIS. JOURNAL OF MAGNETIC RESONANCE IMAGING, 20(5), 765-771.

BASSER, P. J., PAJEVIC, S., PIERPAOLI, C., DUDA, J., & ALDROUBI, A. (2000). IN VIVO FIBER TRACTOGRAPHY USING DT-MRI DATA. MAGNETIC RESONANCE IN MEDICINE, 44(4), 625-632.

BATTAGLINI, M., GIORGIO, A., STROMILLO, M. L., BARTOLOZZI, M. L., GUIDI, L., FEDERICO, A., ET AL. (2009). VOXEL-WISE ASSESSMENT OF PROGRESSION OF REGIONAL BRAIN ATROPHY IN RELAPSING-REMITTING MULTIPLE SCLEROSIS. JOURNAL OF THE NEUROLOGICAL SCIENCES, 282(1), 55-60.

BÖ, L., GEURTS, J. J., VAN DER VALK, P., POLMAN, C., & BARKHOF, F. (2007). LACK OF CORRELATION BETWEEN CORTICAL DEMYELINATION AND WHITE MATTER PATHOLOGIC CHANGES IN MULTIPLE SCLEROSIS. ARCHIVES OF NEUROLOGY, 64(1), 76-80.

BØ, L., VEDELER, C. A., NYLAND, H. I., TRAPP, B. D., & MØRK, S. J. (2003). SUBPIAL DEMYELINATION IN THE CEREBRAL CORTEX OF MULTIPLE SCLEROSIS PATIENTS. JOURNAL OF NEUROPATHOLOGY & EXPERIMENTAL NEUROLOGY, 62(7), 723-732.

BO, L., VEDELER, C. A., NYLAND, H., TRAPP, B. D., & MORK, S. J. (2003). INTRACORTICAL MULTIPLE SCLEROSIS LESIONS ARE NOT ASSOCIATED WITH INCREASED LYMPHOCYTE INFILTRATION. MULTIPLE SCLEROSIS (HOUNDMILLS, BASINGSTOKE, ENGLAND), 9(4), 323-331.

BOAHEN, K. (2000). POINT-TO-POINT CONNECTIVITY BETWEEN NEUROMORPHIC CHIPS USING ADDRESS EVENTS. CIRCUITS AND SYSTEMS II: ANALOG AND DIGITAL SIGNAL PROCESSING, IEEE TRANSACTIONS ON, 47(5), 416-434.

BOZZALI, M., CERCIGNANI, M., SORMANI, M. P., COMI, G., & FILIPPI, M. (2002). QUANTIFICATION OF BRAIN GRAY MATTER DAMAGE IN DIFFERENT MS PHENOTYPES BY USE OF DIFFUSION TENSOR MR IMAGING. AJNR.AMERICAN JOURNAL OF NEURORADIOLOGY, 23(6), 985-988.

BRINK, B. P., VEERHUIS, R., BREIJ, E. C., VAN DER VALK, P., DIJKSTRA, C. D., & BÖ, L. (2005). THE PATHOLOGY OF MULTIPLE SCLEROSIS IS LOCATION-DEPENDENT: NO SIGNIFICANT COMPLEMENT ACTIVATION IS DETECTED IN PURELY CORTICAL LESIONS. JOURNAL OF NEUROPATHOLOGY & EXPERIMENTAL NEUROLOGY, 64(2), 147-155.

BÜRGEL, U., AMUNTS, K., HOEMKE, L., MOHLBERG, H., GILSBACH, J. M., & ZILLES, K. (2006). WHITE MATTER FIBER TRACTS OF THE HUMAN BRAIN: THREE-DIMENSIONAL MAPPING AT MICROSCOPIC RESOLUTION, TOPOGRAPHY AND INTERSUBJECT VARIABILITY. NEUROIMAGE, 29(4), 1092-1105.

CALABRESE, M., AGOSTA, F., RINALDI, F., MATTISI, I., GROSSI, P., FAVARETTO, A., ET AL. (2009). CORTICAL LESIONS AND ATROPHY ASSOCIATED WITH COGNITIVE IMPAIRMENT IN RELAPSING-REMITTING MULTIPLE SCLEROSIS. ARCHIVES OF NEUROLOGY, 66(9), 1144-1150.

CALABRESE, M., MAGLIOZZI, R., CICCARELLI, O., GEURTS, J. J., REYNOLDS, R., & MARTIN, R. (2015). EXPLORING THE ORIGINS OF GREY MATTER DAMAGE IN MULTIPLE SCLEROSIS. NATURE REVIEWS NEUROSCIENCE, 16(3), 147-158.

CATANI, M., & DE SCHOTTEN, M. T. (2008). A DIFFUSION TENSOR IMAGING TRACTOGRAPHY ATLAS FOR VIRTUAL IN VIVO DISSECTIONS. CORTEX, 44(8), 1105-1132.

CATANI, M., & DE SCHOTTEN, M. T. (2008). A DIFFUSION TENSOR IMAGING TRACTOGRAPHY ATLAS FOR VIRTUAL IN VIVO DISSECTIONS. CORTEX, 44(8), 1105-1132.

CATANI, M., DELL'ACQUA, F., BIZZI, A., FORKEL, S. J., WILLIAMS, S. C., SIMMONS, A., ET AL. (2012). BEYOND CORTICAL LOCALIZATION IN CLINICO-ANATOMICAL CORRELATION. CORTEX, 48(10), 1262-1287.

CATANI, M., HOWARD, R. J., PAJEVIC, S., & JONES, D. K. (2002). VIRTUAL IN VIVO INTERACTIVE DISSECTION OF WHITE MATTER FASCICULI IN THE HUMAN BRAIN. NEUROIMAGE, 17(1), 77-94.

CELLE, S., DELON-MARTIN, C., ROCHE, F., BARTHELEMY, J., PÉPIN, J., & DOJAT, M. (2015). DESPERATELY SEEKING GREY MATTER VOLUME CHANGES IN SLEEP APNEA: A METHODOLOGICAL REVIEW OF MAGNETIC RESONANCE BRAIN VOXEL-BASED MORPHOMETRY STUDIES. SLEEP MEDICINE REVIEWS,

CHEE, M. W. L., ZHENG, H., GOH, J. O. S., PARK, D., & SUTTON, B. P. (2011). BRAIN STRUCTURE IN YOUNG AND OLD EAST ASIANS AND WESTERNERS: COMPARISONS OF STRUCTURAL VOLUME AND CORTICAL THICKNESS. JOURNAL OF COGNITIVE NEUROSCIENCE, 23(5), 1065-1079.

DALE, A. M., FISCHL, B., & SERENO, M. I. (1999). CORTICAL SURFACE-BASED ANALYSIS: I. SEGMENTATION AND SURFACE RECONSTRUCTION. NEUROIMAGE, 9(2), 179-194.

DE SCHOTTEN, M. T., BIZZI, A., DELL'ACQUA, F., ALLIN, M., WALSHE, M., MURRAY, R., ET AL. (2011). ATLASING LOCATION, ASYMMETRY AND INTER-SUBJECT VARIABILITY OF WHITE MATTER TRACTS IN THE HUMAN BRAIN WITH MR DIFFUSION TRACTOGRAPHY. NEUROIMAGE, 54(1), 49-59.

DE STEFANO, N., MATTHEWS, P. M., FILIPPI, M., AGOSTA, F., DE LUCA, M., BARTOLOZZI, M. L., ET AL. (2003). EVIDENCE OF EARLY CORTICAL ATROPHY IN MS: RELEVANCE TO WHITE MATTER CHANGES AND DISABILITY. NEUROLOGY, 60(7), 1157-1162.

DICKERSON, B. C., FECZKO, E., AUGUSTINACK, J. C., PACHECO, J., MORRIS, J. C., FISCHL, B., ET AL. (2009). DIFFERENTIAL EFFECTS OF AGING AND ALZHEIMER'S DISEASE ON MEDIAL TEMPORAL LOBE CORTICAL THICKNESS AND SURFACE AREA. NEUROBIOLOGY OF AGING, 30(3), 432-440.

DICKSON, J. W., & GERSTEIN, G. L. (1974). INTERACTIONS BETWEEN NEURONS IN AUDITORY CORTEX OF THE CAT. JOURNAL OF NEUROPHYSIOLOGY, 37(6), 1239-1261.

ELAM, J. S., & VAN ESSEN, D. (2014). HUMAN CONNECTOME PROJECT. ENCYCLOPEDIA OF COMPUTATIONAL NEUROSCIENCE (PP. 1-4) SPRINGER.

EVANGELOU, N., KONZ, D., ESIRI, M. M., SMITH, S., PALACE, J., & MATTHEWS, P. M. (2000). REGIONAL AXONAL LOSS IN THE CORPUS CALLOSUM CORRELATES WITH CEREBRAL WHITE MATTER LESION VOLUME AND DISTRIBUTION IN MULTIPLE SCLEROSIS. BRAIN : A JOURNAL OF NEUROLOGY, 123 (PT 9)(PT 9), 1845-1849.

FISCHL, B., SERENO, M. I., & DALE, A. M. (1999). CORTICAL SURFACE-BASED ANALYSIS: II: INFLATION, FLATTENING, AND A SURFACE-BASED COORDINATE SYSTEM. NEUROIMAGE, 9(2), 195-207.

FISHER, E., LEE, J., NAKAMURA, K., & RUDICK, R. A. (2008). GRAY MATTER ATROPHY IN MULTIPLE SCLEROSIS: A LONGITUDINAL STUDY. ANNALS OF NEUROLOGY, 64(3), 255-265.

FISNIKU, L. K., CHARD, D. T., JACKSON, J. S., ANDERSON, V. M., ALTMANN, D. R., MISZKIEL, K. A., ET AL. (2008). GRAY MATTER ATROPHY IS RELATED TO LONG-TERM DISABILITY IN MULTIPLE SCLEROSIS. ANNALS OF NEUROLOGY, 64(3), 247-254.

FURBY, J., HAYTON, T., ALTMANN, D., BRENNER, R., CHATAWAY, J., SMITH, K. J., ET AL. (2009). DIFFERENT WHITE MATTER LESION CHARACTERISTICS CORRELATE WITH DISTINCT GREY MATTER ABNORMALITIES ON MAGNETIC RESONANCE IMAGING IN SECONDARY PROGRESSIVE MULTIPLE SCLEROSIS. MULTIPLE SCLEROSIS (HOUNDMILLS, BASINGSTOKE, ENGLAND), 15(6), 687-694.

HELLWIG, B. (2000). A QUANTITATIVE ANALYSIS OF THE LOCAL CONNECTIVITY BETWEEN PYRAMIDAL NEURONS IN LAYERS 2/3 OF THE RAT VISUAL CORTEX. BIOLOGICAL CYBERNETICS, 82(2), 111-121.

HENRY, R. G., SHIEH, M., OKUDA, D. T., EVANGELISTA, A., GORNO-TEMPINI, M. L., & PELLETIER, D. (2008). REGIONAL GREY MATTER ATROPHY IN CLINICALLY ISOLATED SYNDROMES AT PRESENTATION. JOURNAL OF NEUROLOGY, NEUROSURGERY, AND PSYCHIATRY, 79(11), 1236-1244.

HORAKOVA, D., COX, J. L., HAVRDOVA, E., HUSSEIN, S., DOLEZAL, O., COOKFAIR, D., ET AL. (2008). EVOLUTION OF DIFFERENT MRI MEASURES IN PATIENTS WITH ACTIVE RELAPSING-REMITTING MULTIPLE SCLEROSIS OVER 2 AND 5 YEARS: A CASE-CONTROL STUDY. JOURNAL OF NEUROLOGY, NEUROSURGERY, AND PSYCHIATRY, 79(4), 407-414.

HUERTA, M. F., KOSLOW, S. H., & LESHNER, A. I. (1993). THE HUMAN BRAIN PROJECT: AN INTERNATIONAL RESOURCE. TRENDS IN NEUROSCIENCES, 16(11), 436-438.

HULST, H. E., & GEURTS, J. J. (2011). GRAY MATTER IMAGING IN MULTIPLE SCLEROSIS: WHAT HAVE WE LEARNED? BMC NEUROLOGY, 11, 153-2377-11-153.

JEHNA, M., PIRPAMER, L., KHALIL, M., FUCHS, S., ROPELE, S., LANGKAMMER, C., ET AL. (2015). PERIVENTRICULAR LESIONS CORRELATE WITH CORTICAL THINNING IN MULTIPLE SCLEROSIS. ANNALS OF NEUROLOGY, 78(4), 530-539.

JURE, L., ZAARAOUI, W., ROUSSEAU, C., REUTER, F., RICO, A., MALIKOVA, I., ET AL. (2010). INDIVIDUAL VOXEL-BASED ANALYSIS OF BRAIN MAGNETIZATION TRANSFER MAPS SHOWS GREAT VARIABILITY OF GRAY MATTER INJURY IN THE FIRST STAGE OF MULTIPLE SCLEROSIS. JOURNAL OF MAGNETIC RESONANCE IMAGING, 32(2), 424-428.

KLAVER, R., DE VRIES, H. E., SCHENK, G. J., & GEURTS, J. J. GREY MATTER DAMAGE IN MULTIPLE SCLEROSIS.

KOLASINSKI, J., STAGG, C. J., CHANCE, S. A., DELUCA, G. C., ESIRI, M. M., CHANG, E. H., ET AL. (2012). A COMBINED POST-MORTEM MAGNETIC RESONANCE IMAGING AND QUANTITATIVE HISTOLOGICAL STUDY OF MULTIPLE SCLEROSIS PATHOLOGY. BRAIN : A JOURNAL OF NEUROLOGY, 135(PT 10), 2938-2951.

KOSLOW, S. H., & HUERTA, M. F. (1997). NEUROINFORMATICS: AN OVERVIEW OF THE HUMAN BRAIN PROJECT PSYCHOLOGY PRESS.

LAISNEY, M., GIFFARD, B., BELLIARD, S., DE LA SAYETTE, V., DESGRANGES, B., & EUSTACHE, F. (2011). WHEN THE ZEBRA LOSES ITS STRIPES: SEMANTIC PRIMING IN EARLY ALZHEIMER'S DISEASE AND SEMANTIC DEMENTIA. CORTEX, 47(1), 35-46.

LASSMANN, H. (2012). CORTICAL LESIONS IN MULTIPLE SCLEROSIS: INFLAMMATION VERSUS NEURODEGENERATION. BRAIN : A JOURNAL OF NEUROLOGY, 135(PT 10), 2904-2905.

LAWES, I. N. C., BARRICK, T. R., MURUGAM, V., SPIERINGS, N., EVANS, D. R., SONG, M., ET AL. (2008). ATLAS-BASED SEGMENTATION OF WHITE MATTER TRACTS OF THE HUMAN BRAIN USING DIFFUSION TENSOR TRACTOGRAPHY AND COMPARISON WITH CLASSICAL DISSECTION. NEUROIMAGE, 39(1), 62-79.

LIU, Y., DUAN, Y., HE, Y., YU, C., WANG, J., HUANG, J., ET AL. (2012). WHOLE BRAIN WHITE MATTER CHANGES REVEALED BY MULTIPLE DIFFUSION METRICS IN MULTIPLE SCLEROSIS: A TBSS STUDY. EUROPEAN JOURNAL OF RADIOLOGY, 81(10), 2826-2832.

MAKRIS, N., WORTH, A., PAPADIMITRIOU, G., STAKES, J., CAVINESS, V., KENNEDY, D., ET AL. (1997). MORPHOMETRY OF IN VIVO HUMAN WHITE MATTER ASSOCIATION PATHWAYS WITH DIFFUSION-WEIGHTED MAGNETIC RESONANCE IMAGING. ANNALS OF NEUROLOGY, 42(6), 951-962.

MAMAH, D., CONTURO, T. E., HARMS, M. P., AKBUDAK, E., WANG, L., MCMICHAEL, A. R., ET AL. (2010). ANTERIOR THALAMIC RADIATION INTEGRITY IN SCHIZOPHRENIA: A DIFFUSION-TENSOR IMAGING STUDY. PSYCHIATRY RESEARCH: NEUROIMAGING, 183(2), 144-150.

MELHEM, E. R., MORI, S., MUKUNDAN, G., KRAUT, M. A., POMPER, M. G., & VAN ZIJL, P. C. (2002). DIFFUSION TENSOR MR IMAGING OF THE BRAIN AND WHITE MATTER TRACTOGRAPHY. AMERICAN JOURNAL OF ROENTGENOLOGY, 178(1), 3-16.

MICHALSKI, A., GERSTEIN, G., CZARKOWSKA, J., & TARNECKI, R. (1983). INTERACTIONS BETWEEN CAT STRIATE CORTEX NEURONS. EXPERIMENTAL BRAIN RESEARCH, 51(1), 97-107.

MISTRY, N., ABDEL-FAHIM, R., MOUGIN, O., TENCH, C., GOWLAND, P., & EVANGELOU, N. (2014). CORTICAL LESION LOAD CORRELATES WITH DIFFUSE INJURY OF MULTIPLE SCLEROSIS NORMAL APPEARING WHITE MATTER. MULTIPLE SCLEROSIS (HOUNDMILLS, BASINGSTOKE, ENGLAND), 20(2), 227-233.

NARAYANA, P. A., GOVINDARAJAN, K. A., GOEL, P., DATTA, S., LINCOLN, J. A., COFIELD, S. S., ET AL. (2013). REGIONAL CORTICAL THICKNESS IN RELAPSING REMITTING MULTIPLE SCLEROSIS: A MULTI-CENTER STUDY. NEUROIMAGE: CLINICAL, 2, 120-131.

NYGAARD, G. O., WALHOVD, K. B., SOWA, P., CHEPKOECH, J. L., BJORNERUD, A., DUE-TONNESSEN, P., ET AL. (2015). CORTICAL THICKNESS AND SURFACE AREA RELATE TO SPECIFIC SYMPTOMS IN EARLY RELAPSING-REMITTING MULTIPLE SCLEROSIS. MULTIPLE SCLEROSIS (HOUNDMILLS, BASINGSTOKE, ENGLAND), 21(4), 402-414.

OH, J. S., KUBICKI, M., ROSENBERGER, G., BOUIX, S., LEVITT, J. J., MCCARLEY, R. W., ET AL. (2009). THALAMO-FRONTAL WHITE MATTER ALTERATIONS IN CHRONIC SCHIZOPHRENIA. HUMAN BRAIN MAPPING, 30(11), 3812-3825.

PAPAGNO, C., MIRACAPILLO, C., CASAROTTI, A., ROMERO LAURO, L. J., CASTELLANO, A., FALINI, A., ET AL. (2011). WHAT IS THE ROLE OF THE UNCINATE FASCICULUS? SURGICAL REMOVAL AND PROPER NAME RETRIEVAL. BRAIN : A JOURNAL OF NEUROLOGY, 134(PT 2), 405-414.

PARETO, D., SASTRE-GARRIGA, J., AUGER, C., VIVES-GILABERT, Y., DELGADO, J., TINTORÉ, M., ET AL. (2015). JUXTACORTICAL LESIONS AND CORTICAL THINNING IN MULTIPLE SCLEROSIS. AMERICAN JOURNAL OF NEURORADIOLOGY,

POPESCU, B. F., & LUCCHINETTI, C. F. (2012). MENINGEAL AND CORTICAL GREY MATTER PATHOLOGY IN MULTIPLE SCLEROSIS. BMC NEUROLOGY, 12, 11-2377-12-11.

POPESCU, V., KLAVER, R., VOORN, P., GALIS-DE GRAAF, Y., KNOL, D. L., TWISK, J. W., ET AL. (2015). WHAT DRIVES MRI-MEASURED CORTICAL ATROPHY IN MULTIPLE SCLEROSIS? MULTIPLE SCLEROSIS (HOUNDMILLS, BASINGSTOKE, ENGLAND), 21(10), 1280-1290.

RIMRODT, S. L., PETERSON, D. J., DENCKLA, M. B., KAUFMANN, W. E., & CUTTING, L. E. (2010). WHITE MATTER MICROSTRUCTURAL DIFFERENCES LINKED TO LEFT PERISYLVIAN LANGUAGE NETWORK IN CHILDREN WITH DYSLEXIA. CORTEX, 46(6), 739-749.

ROOSENDAAL, S. D., BENDFELDT, K., VRENKEN, H., POLMAN, C. H., BORGWARDT, S., RADUE, E. W., ET AL. (2011). GREY MATTER VOLUME IN A LARGE COHORT OF MS PATIENTS: RELATION TO MRI PARAMETERS AND DISABILITY. MULTIPLE SCLEROSIS (HOUNDMILLS, BASINGSTOKE, ENGLAND), 17(9), 1098-1106.

ROVARIS, M., CONFAVREUX, C., FURLAN, R., KAPPOS, L., COMI, G., & FILIPPI, M. (2006). SECONDARY PROGRESSIVE MULTIPLE SCLEROSIS: CURRENT KNOWLEDGE AND FUTURE CHALLENGES. THE LANCET NEUROLOGY, 5(4), 343-354.

RUBINOV, M., & SPORNS, O. (2010). COMPLEX NETWORK MEASURES OF BRAIN CONNECTIVITY: USES AND INTERPRETATIONS. NEUROIMAGE, 52(3), 1059-1069.

SAILER, M., FISCHL, B., SALAT, D., TEMPELMANN, C., SCHONFELD, M. A., BUSA, E., ET AL. (2003). FOCAL THINNING OF THE CEREBRAL CORTEX IN MULTIPLE SCLEROSIS. BRAIN : A JOURNAL OF NEUROLOGY, 126(PT 8), 1734-1744.

SAMESHIMA, K., & BACCALÁ, L. A. (1999). USING PARTIAL DIRECTED COHERENCE TO DESCRIBE NEURONAL ENSEMBLE INTERACTIONS. JOURNAL OF NEUROSCIENCE METHODS, 94(1), 93-103.

SBARDELLA, E., TONA, F., PETSAS, N., & PANTANO, P. (2013). DTI MEASUREMENTS IN MULTIPLE SCLEROSIS: EVALUATION OF BRAIN DAMAGE AND CLINICAL IMPLICATIONS. MULTIPLE SCLEROSIS INTERNATIONAL, 2013, 671730.

SCARPAZZA, C., TOGNIN, S., FRISCIATA, S., SARTORI, G., & MECHELLI, A. (2015). FALSE POSITIVE RATES IN VOXEL-BASED MORPHOMETRY STUDIES OF THE HUMAN BRAIN: SHOULD WE BE WORRIED? NEUROSCIENCE & BIOBEHAVIORAL REVIEWS, 52, 49-55.

SEPULCRE, J., GOÑI, J., MASDEU, J. C., BEJARANO, B., DE MENDIZÁBAL, N. V., TOLEDO, J. B., ET AL. (2009). CONTRIBUTION OF WHITE MATTER LESIONS TO GRAY MATTER ATROPHY IN MULTIPLE SCLEROSIS: EVIDENCE FROM VOXEL-BASED ANALYSIS OF T1 LESIONS IN THE VISUAL PATHWAY. ARCHIVES OF NEUROLOGY, 66(2), 173-179.

SHEPHERD, G. M., MIRSKY, J. S., HEALY, M. D., SINGER, M. S., SKOUFOS, E., HINES, M. S., ET AL. (1998). THE HUMAN BRAIN PROJECT: NEUROINFORMATICS TOOLS FOR INTEGRATING, SEARCHING AND MODELING MULTIDISCIPLINARY NEUROSCIENCE DATA. TRENDS IN NEUROSCIENCES, 21(11), 460-468.

SHINOURA, N., SUZUKI, Y., TSUKADA, M., KATSUKI, S., YAMADA, R., TABEI, Y., ET AL. (2007). IMPAIRMENT OF INFERIOR LONGITUDINAL FASCICULUS PLAYS A ROLE IN VISUAL MEMORY DISTURBANCE. NEUROCASE, 13(2), 127-130.

SPORNS, O., TONONI, G., & EDELMAN, G. (2002). THEORETICAL NEUROANATOMY AND THE CONNECTIVITY OF THE CEREBRAL CORTEX. BEHAVIOURAL BRAIN RESEARCH, 135(1), 69-74.

SPORNS, O., CHIALVO, D. R., KAISER, M., & HILGETAG, C. C. (2004). ORGANIZATION, DEVELOPMENT AND FUNCTION OF COMPLEX BRAIN NETWORKS. TRENDS IN COGNITIVE SCIENCES, 8(9), 418-425.

STEENWIJK, M. D., DAAMS, M., POUWELS, P. J., J BALK, L., TEWARIE, P. K., GEURTS, J. J., ET AL. (2015). UNRAVELING THE RELATIONSHIP BETWEEN REGIONAL GRAY MATTER ATROPHY AND PATHOLOGY IN CONNECTED WHITE MATTER TRACTS IN LONG-STANDING MULTIPLE SCLEROSIS. HUMAN BRAIN MAPPING, 36(5), 1796-1807.

STEENWIJK, M. D., POUWELS, P. J., DAAMS, M., VAN DALEN, J. W., CAAN, M. W., RICHARD, E., ET AL. (2013). ACCURATE WHITE MATTER LESION SEGMENTATION BY K NEAREST NEIGHBOR CLASSIFICATION WITH TISSUE TYPE PRIORS (KNN-TTPS). NEUROIMAGE: CLINICAL, 3, 462-469.

TEDESCHI, G., DINACCI, D., COMERCI, M., LAVORGNA, L., SAVETTIERI, G., QUATTRONE, A., ET AL. (2009). BRAIN ATROPHY EVOLUTION AND LESION LOAD ACCRUAL IN MULTIPLE SCLEROSIS: A 2-YEAR FOLLOW-UP STUDY. MULTIPLE SCLEROSIS (HOUNDMILLS, BASINGSTOKE, ENGLAND), 15(2), 204-211.

TEDESCHI, G., LAVORGNA, L., RUSSO, P., PRINSTER, A., DINACCI, D., SAVETTIERI, G., ET AL. (2005). BRAIN ATROPHY AND LESION LOAD IN A LARGE POPULATION OF PATIENTS WITH MULTIPLE SCLEROSIS. NEUROLOGY, 65(2), 280-285.

THOMAS, J. B., & WYMAN, R. J. (1984). MUTATIONS ALTERING SYNAPTIC CONNECTIVITY BETWEEN IDENTIFIED NEURONS IN DROSOPHILA. THE JOURNAL OF NEUROSCIENCE : THE OFFICIAL JOURNAL OF THE SOCIETY FOR NEUROSCIENCE, 4(2), 530-538.

VAN ESSEN, D. C., UGURBIL, K., AUERBACH, E., BARCH, D., BEHRENS, T., BUCHOLZ, R., ET AL. (2012). THE HUMAN CONNECTOME PROJECT: A DATA ACQUISITION PERSPECTIVE. NEUROIMAGE, 62(4), 2222-2231.

VAN HORSSEN, J., BRINK, B. P., DE VRIES, H. E., VAN DER VALK, P., & BO, L. (2007). THE BLOOD-BRAIN BARRIER IN CORTICAL MULTIPLE SCLEROSIS LESIONS. JOURNAL OF NEUROPATHOLOGY AND EXPERIMENTAL NEUROLOGY, 66(4), 321-328.

WATKINS, K. E., SMITH, S. M., DAVIS, S., & HOWELL, P. (2008). STRUCTURAL AND FUNCTIONAL ABNORMALITIES OF THE MOTOR SYSTEM IN DEVELOPMENTAL STUTTERING. BRAIN : A JOURNAL OF NEUROLOGY, 131(PT 1), 50-59.

WINKLER, A. M., SABUNCU, M. R., YEO, B. T., FISCHL, B., GREVE, D. N., KOCHUNOV, P., ET AL. (2012). MEASURING AND COMPARING BRAIN CORTICAL SURFACE AREA AND OTHER AREAL QUANTITIES. NEUROIMAGE, 61(4), 1428-1443.

YENDIKI, A., PANNECK, P., SRINIVASAN, P., STEVENS, A., ZOLLEI, L., AUGUSTINACK, J., ET AL. (2011). AUTOMATED PROBABILISTIC RECONSTRUCTION OF WHITE-MATTER PATHWAYS IN HEALTH AND DISEASE USING AN ATLAS OF THE UNDERLYING ANATOMY. FRONTIERS IN NEUROINFORMATICS, 5, 23.

ZIVADINOV, R., & PIRKO, I. (2012). ADVANCES IN UNDERSTANDING GRAY MATTER PATHOLOGY IN MULTIPLE SCLEROSIS: ARE WE READY TO REDEFINE DISEASE PATHOGENESIS? BMC NEUROLOGY, 12, 9-2377-12-9.